RESEARCH ARTICLE SUMMARY

CHEMICAL BIOLOGY

Multiscale photocatalytic proximity labeling reveals cell surface neighbors on and between cells

Zhi Lin, Kaitlin Schaefer, Irene Lui, Zi Yao, Andrea Fossati, Danielle L. Swaney, Ajikarunia Palar, Andrej Sali, James A. Wells*

INTRODUCTION: The cell membrane proteome is the primary biohub for cell communication, yet we are only beginning to understand the dynamic protein neighborhoods and their functions on the cell surface and between cells. Proximity labeling proteomics (PLP) is a powerful approach for identifying transient protein interactomes in situ and is crucial for therapeutic target discovery and protein functional studies. First-generation proximity labeling methods such as APEX and BioID used enzymatic catalysis and required cellular engineering. They provided interactome maps with broad spatial resolution (up to 3000 Å) owed to the long reactive half-lives of the probes. Recently developed photocatalytic proximity labeling, such as μMap, provides an alternative strategy with an enhanced resolution (~100 Å) by using a highly reactive diazirine probe. However, current PLP methods are limited to one single resolution based on the probe of choice and its labeling radius. No single method can cover all the labeling length scales, and thus, users need to switch between these proximity labeling methods to interrogate different biological systems.

RATIONALE: To identify protein interactome with high confidence, we demonstrated a new PLP platform named MultiMap that enables facile interactome profiling with an adjustable resolution and integrated target validation workflow. MultiMap relies on the discovery of a single organic photocatalyst, Eosin Y, that activates all major types of photo-probes—diazirine, aryl-azide, and phenol—each with a different labeling radius. This commercially available photocatalyst can be conjugated to antibodies of interest through facile bioconjugation, allowing us to capture and visualize protein neighborhoods without extensive protein engineering both on and between cells.

RESULTS: MultiMap enabled us to explore the neighborhoods of an important therapeutic node in oncology, epidermal growth factor receptor (EGFR). Using a facile two-step bioconjugation method to incorporate Eosin Y onto antibodies, we identified more than 20 neighbors of high confidence, most of which were previously unidentified. These neighbors included a phosphatase, multiple stabilizing proteins, and EGFR substrates that have been functionally associated but not structurally shown to connect. In addition, by introducing in silico binary interaction prediction with AlphaFold-Multimer as a new part of the integrated proximity profiling workflow, plausible and testable structural models of the important therapeutic neighborhood surrounding EGFR were further provided. MultiMap was also expanded to map intercellular neighborhoods where four different cell-cell synapses induced by therapeutic modalities that include bispecific T cell engagers (BiTEs) and a chimeric antigen receptor (CAR) were showcased. We confirmed that MultiMap can label both contacting cells and neighbor proteins with high selectivity, which can be generalizable for different synaptic discoveries.

CONCLUSION: We developed a multiscale PLP method for interactome profiling on the cell surface and between cells. Across these different biological scenarios, MultiMap is a highly versatile and adaptable platform to study interactomes. It provides a wealth of neighborhood information of high and low resolution using one photocatalyst, one workflow, and minimal protein engineering. MultiMap substantially streamlines the photocatalytic PLP workflow. We envision that this platform will accelerate future interactome studies, allowing us to better understand horizontal signaling on the membrane. ■

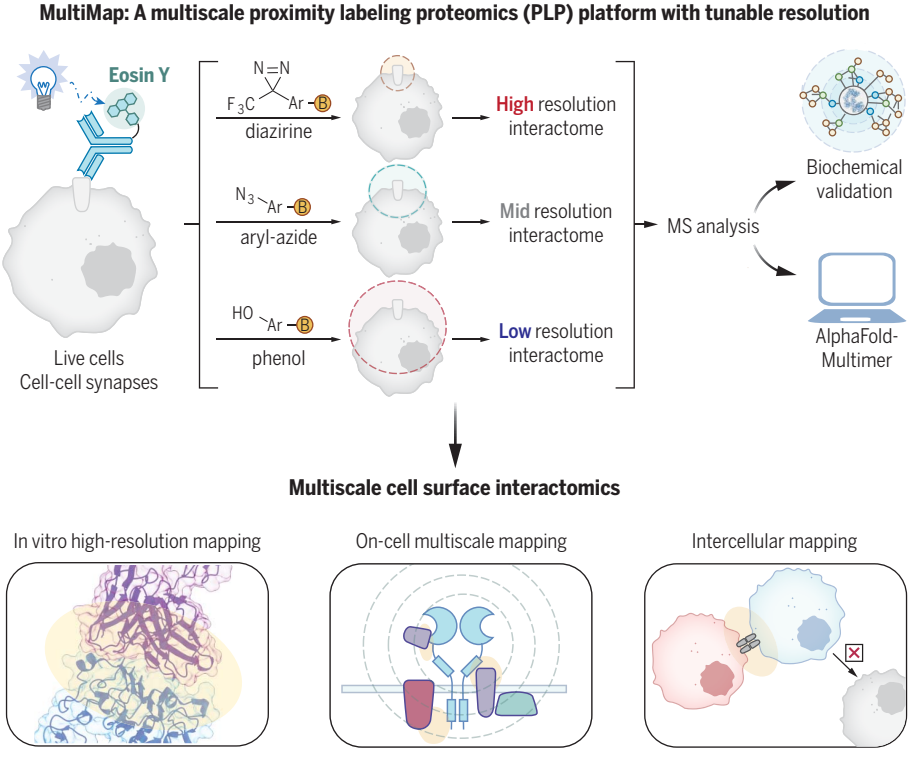

High-resolution interactome mapping by using a multiscale photocatalytic proximity labeling method. We developed MultiMap, a multiscale PLP platform that allows the capturing of protein neighborhoods on and between cells. By using one single commercially available photocatalyst, Eosin Y, we obtained high-, mid-, and low-resolution neighborhoods using photo-probes with different labeling radii and characterized the interacting partners through an integrated workflow of biochemical immunoassays and AlphaFold-Multimer structure prediction. This multiscale cell surface interactomics platform is also capable of capturing the synaptic neighborhood formed between interacting cells.

The list of author affiliations is available in the full article online.
*Corresponding author. Email: jim.wells@ucsf.edu
Cite this article as Z. Lin *et al.*, *Science* **385**, eadl5763 (2024).
DOI: 10.1126/science.adl5763

READ THE FULL ARTICLE AT
https://doi.org/10.1126/science.adl5763

RESEARCH ARTICLE

CHEMICAL BIOLOGY

Multiscale photocatalytic proximity labeling reveals cell surface neighbors on and between cells

Zhi Lin[1], Kaitlin Schaefer[1], Irene Lui[1], Zi Yao[1], Andrea Fossati[2,3,4], Danielle L. Swaney[2,3,4], Ajikarunia Palar[1,3,5], Andrej Sali[1,3,5], James A. Wells[1,2]*

Proximity labeling proteomics (PLP) strategies are powerful approaches to yield snapshots of protein neighborhoods. Here, we describe a multiscale PLP method with adjustable resolution that uses a commercially available photocatalyst, Eosin Y, which upon visible light illumination activates different photo-probes with a range of labeling radii. We applied this platform to profile neighborhoods of the oncogenic epidermal growth factor receptor and orthogonally validated more than 20 neighbors using immunoassays and AlphaFold-Multimer prediction. We further profiled the protein neighborhoods of cell-cell synapses induced by bispecific T cell engagers and chimeric antigen receptor T cells. This integrated multiscale PLP platform maps local and distal protein networks on and between cell surfaces, which will aid in the systematic construction of the cell surface interactome, revealing horizontal signaling partners and reveal new immunotherapeutic opportunities.

Cell surface proteins are critical mediators of information, nutrients, and functions on cells and between them. The extracellular proteome, both secreted and membrane-bound, is encoded by more than 25% of the human genome (*1*, *2*). Proteomics methods have made great strides in characterizing the composition of the surface proteome in health and disease models (*3*, *4*). However, we know much less about the protein-protein interactions formed on the cell membrane, especially transient interactions that regulate cell signaling networks.

Proximity labeling proteomics (PLP) methods have enabled the identification of protein interactomes in complex cellular environments (*5*, *6*). These methods typically generate a single reactive intermediate locally to label and profile nearby proteins by use of imaging or proteomics. The first generation of PLP methods used genetically encoded enzymes such as APEX (*7*), BioID (*8*), or TurboID (*9*, *10*) to produce phenoxyl radicals or activated adenosine 5′-monophosphate (AMP) that have long reactive half-lives ($t_{1/2}$ > 100 μs). These methods are well suited for characterizing cell-cell and organelle-specific interactomes given their long labeling range of up to 3000 Å by labeling electron-rich amino acids (*11*). Singlet oxygen generators (SOGs) trigger selective labeling on histidine (*12*) at a shorter range given the shorter half-life of singlet oxygen in water (~2 to 4 μs) (*13*). However, proteins are estimated to be separated by only 60 to 70 Å on the crowded cell surface (*14*), thus making it challenging to identify the most proximal protein neighbors with long-range PLP approaches.

Most recently, PLP methods of very short range have emerged, enabling higher-resolution mapping, including μMap (*15*–*18*). These designs use transition metals or other photocatalysts attached to antibodies to trigger reactive intermediates with shorter half-lives such as carbenes or nitrenes ($t_{1/2}$ = ~2 and 10 ns, respectively) (*11*, *19*). Activation of these probes enables labeling proteins at a much shorter range of ~100 to 700 Å as well as broader amino acid coverage (*11*, *20*), thus making it much more appropriate for nearest-neighborhood analysis (*21*–*24*). Collectively, the suite of PLP methods can cover a broad length scale for labeling protein neighborhoods and synapses but require multiple photocatalysts for adjustable resolution.

Here, we report a multiscale photocatalytic PLP technology, termed MultiMap (Fig. 1A), that allows short-, intermediate-, and long-range labeling from a single photocatalyst, Eosin Y (EY). We discovered that EY, a fluorescent dye commonly used in food chemistry and biological staining (*21*), can efficiently trigger the labeling by using diazirine, aryl-azide, and phenol photo-probes with biocompatible blue or green light. We applied MultiMap to profile high-resolution neighborhoods of the oncogenic epidermal growth factor receptor (EGFR) in different cellular contexts. We identified more than 20 neighbors and further validated their interactions through immunoprecipitation and in silico prediction models using AlphaFold-Multimer (*25*). We demonstrated that MultiMap can capture long-range intercellular engagements between cancer cells and T lymphocytes induced by bispecific T cell engagers (BiTEs) and engineered chimeric antigen receptors (CARs). Our data show that MultiMap is an effective multiscale PLP technology that can characterize local and distal cellular interactomes from a single photocatalyst. We believe that with artificial intelligence–assisted structural prediction methods integrated, the MultiMap workflow will be an important approach in the broad quest to define the spatial organization of the cell surface proteome.

EY activates a panel of photo-probes for protein labeling

We explored EY for PLP (Fig. 1A and fig. S1A) on the basis of its photocatalytic ability broadly used in polymer synthesis (*26*) and easy commercial access (*27*). By contrast, the current transition-metal photocatalysts used in μMap, such as the iridium (Ir) catalyst (fig. S1A), requires lengthy synthetic routes (*15*, *28*). We first tested the ability of EY to label bovine serum albumin (BSA) using a diazirine-biotin probe in the presence of light (Fig. 1B and fig. S1B). We observed time- and light-dependent accumulation of biotinylated BSA by means of Western blot (WB) analysis; labeling plateaued within 6 min of blue light-emitting diode (LED) illumination (Fig. 1B, left). A pulse-light experiment (Fig. 1B, right) demonstrated that the catalytic function of EY is light dependent. Parallel comparison of EY-activated BSA biotinylation showed much higher signal than background with 2 and 10 min of illumination (fig. S1C).

EY is structurally similar to other photosensitizers that can either trigger labeling using aryl-azide and phenol probes or induce singlet oxygen–based labeling using biocytin-hydrazide (*12*, *27*, *29*, *30*). We tested the photocatalytic labeling on BSA and found that EY efficiently catalyzed biotin labeling in the presence of aryl-azide-biotin, biocytin-hydrazide, or phenol-biotin (Fig. 1C and fig. S1D). The extents of BSA labeling by using soluble EY among the four biotin-containing reactive probes, which we refer to as photo-probes, ranged in the following order: aryl-azide-biotin (>95%), biocytin-hydrazide (>90%), phenol-biotin (~40%), and diazirine-biotin (~5%) (fig. S1D). Under blue light illumination, the Ir catalyst could trigger labeling of BSA by the aryl-azide-biotin but not the phenol-biotin (fig. S1D).

The absorption peak for EY (λ_{max} = 517 nm) (fig. S1E) was also red-shifted compared with the Ir catalyst (λ_{max} = 420 nm) (*15*), which could make EY more biocompatible given the potential toxicity of blue light (*31*). A closer

[1]Department of Pharmaceutical Chemistry, University of California, San Francisco, San Francisco, CA 94158, USA. [2]Department of Cellular and Molecular Pharmacology, University of California, San Francisco, San Francisco, CA 94158, USA. [3]Quantitative Biosciences Institute, University of California, San Francisco, San Francisco, CA 94158, USA. [4]J. David Gladstone Institute of Data Science and Biotechnology, Gladstone Institutes, San Francisco, CA 94158, USA. [5]Department of Bioengineering and Therapeutic Sciences, University of California, San Francisco, San Francisco, CA 94158, USA.
*Corresponding author. Email: jim.wells@ucsf.edu

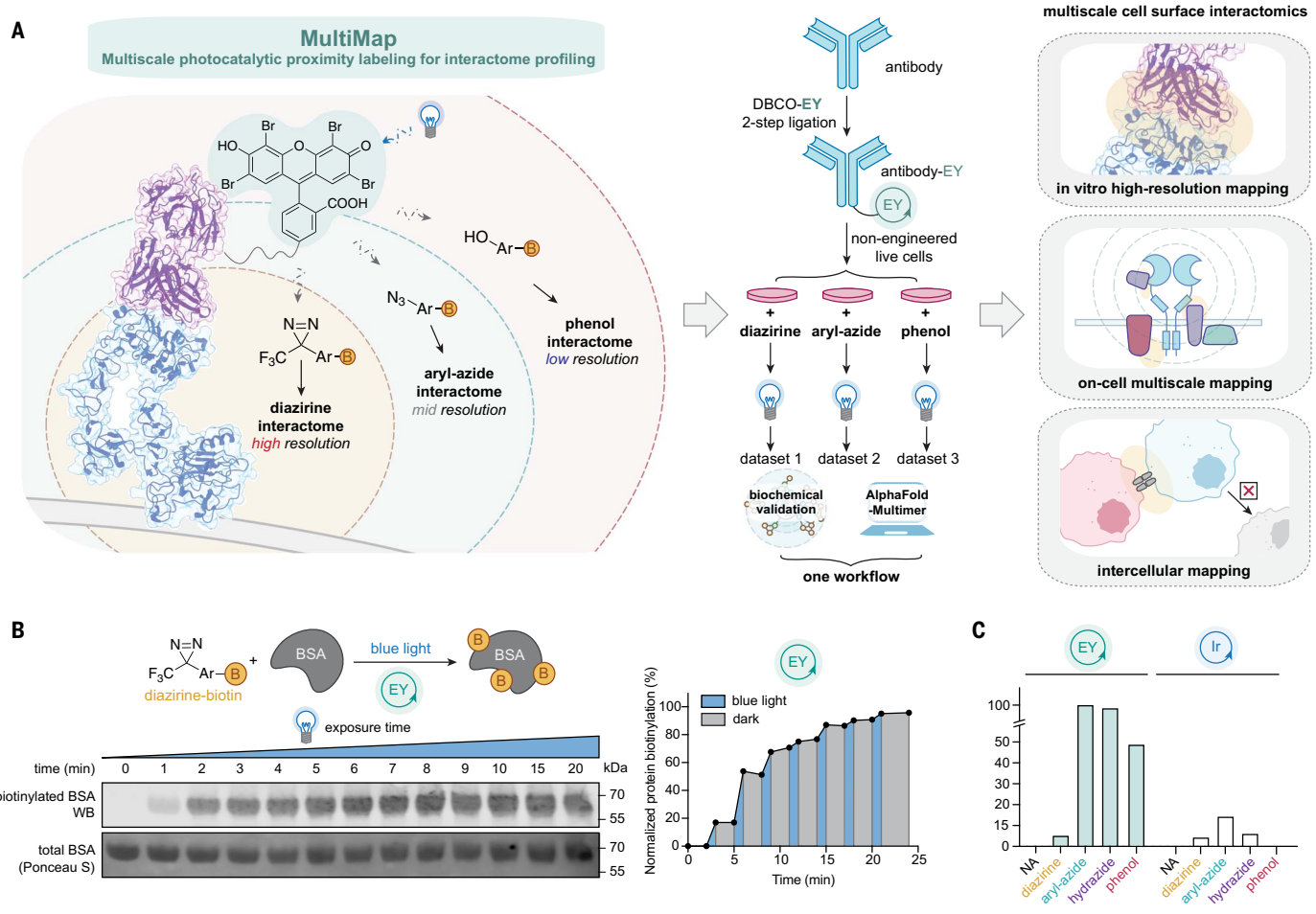

Fig. 1. MultiMap captures high-resolution snapshots of biological networks across a wide range of length scales. (**A**) A schematic of the MultiMap workflow. EY is conjugated to an antibody that binds the target of interest (for example, Fab arm of Ctx bound to the EGFR extracellular domain). Upon illumination, proteins are biotinylated, captured, and digested for MS analysis. Proteomic hits are further examined by means of immunoprecipitation and predictive structural analysis with AlphaFold-Multimer. MultiMap is a useful platform for profiling local membrane protein interactomes both on live cells and between cell-cell synapses. (**B**) WB showing EY-mediated photocatalytic biotinylation of BSA by a diazirine-biotin probe upon blue LED illumination. Biotinylation can be controlled temporally with pulsed light. (**C**) EY triggers labeling of BSA with four photo-probes (diazirine-biotin, aryl-azide-biotin, biocytin-hydrazide, and phenol-biotin).

examination of biotinylation efficiency in a time-course experiment demonstrated that EY indeed efficiently catalyzed labeling of BSA with green LED (λ = 525 nm), whereas the Ir catalyst showed no labeling (fig. S2, A and B). More than 80% labeling of BSA was achieved upon 3 min of green LED exposure of EY with all four photo-probes. We also found that EY maintains its photocatalytic function above its pK_a (pH = 3.5) (fig. S2, C and D) (*27*) and thus is compatible with labeling across a wide range of physiological pH conditions.

Conjugation of EY onto proteins

We evaluated different conjugation methods for EY first onto BSA and then to antibodies (Fig. 2A and fig. S3A). After synthesizing dibenzocyclooctyne (DBCO)–PEG_4-EY through an amine-isothiocyanate reaction (scheme S1), we explored the conjugation efficiency and stoichiometry for attaching a click-compatible azido functionality specifically to Lys, Met, or Cys using *N*-hydroxy succinimide (NHS) ester, oxaziridine, or maleimide or iodoacetamide warheads, respectively (fig. S3B) (*32*). EY-conjugation through NHS-azide ligation produced the most efficient conjugation; conjugated EY also efficiently catalyzed BSA self-biotinylation with diazirine-biotin, aryl-azide-biotin, and phenol-biotin (fig. S3, B and C).

Next, we conjugated EY to cetuximab (Ctx), an US Food and Drug Administration–approved antibody that selectively binds EGFR and competes for epidermal growth factor (EGF) binding, thus turning off EGFR signaling and cell proliferation in cancer (Fig. 2B) (*33*, *34*). Ctx does not have Lys, Met, or Cys residues in the complementarity-determining regions (CDRs) or in the contact epitope with the EGFR ectodomain [ECD; amino acids 1 to 645, Protein Data Bank (PDB) ID 1YY9] (*33*), suggesting all bioconjugation methods are viable without impairing binding. We tested the same panel of bioconjugation warheads on Ctx, generating levels of conjugation similar to those seen for BSA (fig. S3D). Quantification of the levels of conjugation by means of WB analysis or EY absorption indicated that a stoichiometry of eight and two EY catalysts were installed per Ctx-NHS-EY and Ctx-Ox-EY, respectively (fig. S3, E and F).

We then tested the intra- and intermolecular labeling of the Ctx-EY conjugates with recombinant human EGFR ECD and in competition with EGF (Fig. 2C). Upon blue LED illumination, both Ctx-NHS-EY and Ctx-Ox-EY conjugates demonstrated self-labeling in a light-dependent manner. Not surprisingly, there was a higher degree of biotinylation with Ctx-NHS-EY, which contains approximately four-fold more conjugated EY than that in Ctx-Ox-EY (fig. S3D). Intermolecular EGFR labeling with both EY-conjugated constructs occurred in a

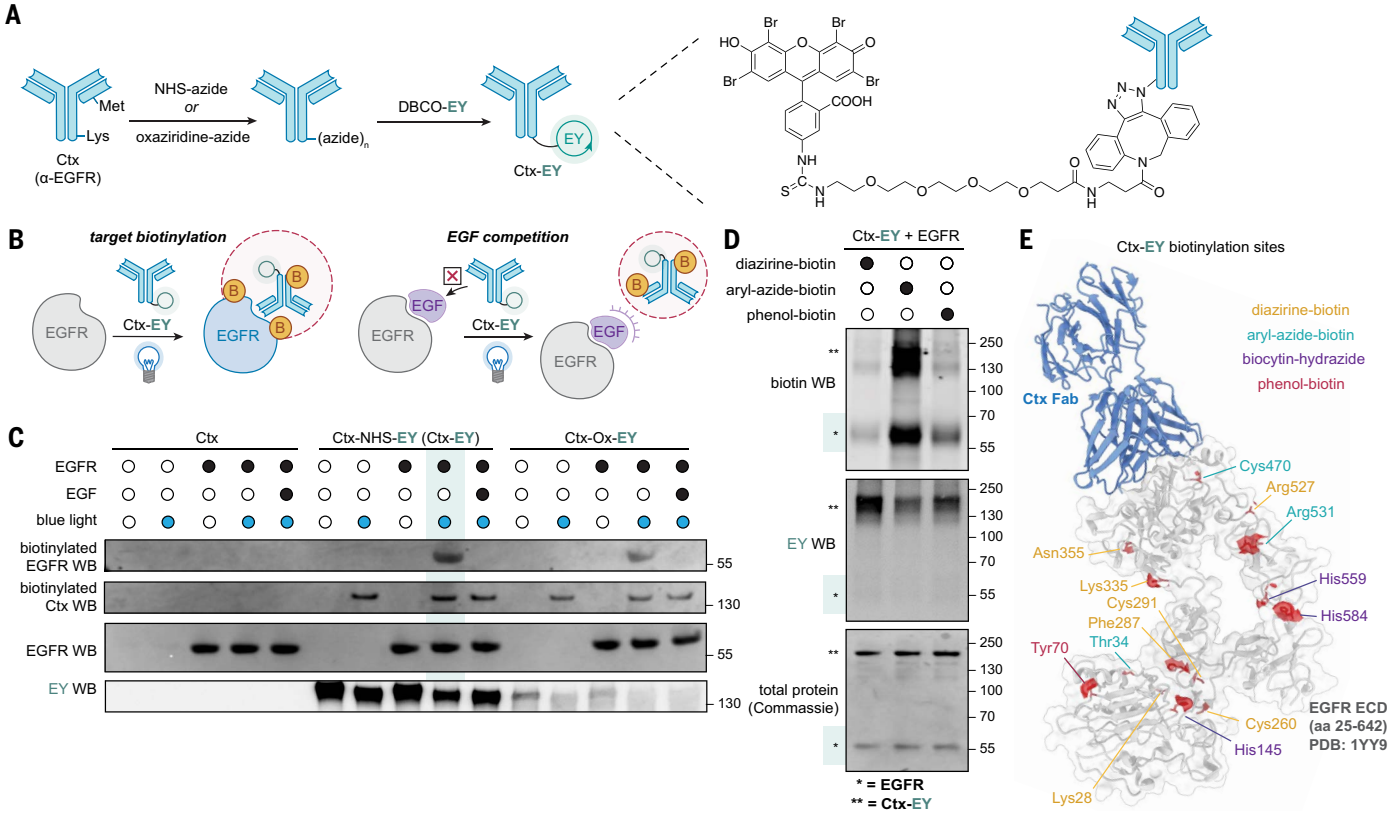

Fig. 2. Targeted labeling using antibody-EY conjugates in vitro. (**A**) Synthetic scheme of Ctx-EY through a two-step bioconjugation workflow. An azido functionality was first introduced onto either Lys or Met residues by using NHS or oxaziridine chemistry, respectively, followed by bio-orthogonal click reaction to couple EY. (**B**) Schematic design to test intra- and interbiotinylation of Ctx-EY and EGFR with or without EGF competition. (**C**) Targeted EGFR biotinylation with the diazirine-biotin photo-probe when triggered by either Ctx-NHS-EY (Ctx-EY) or Ctx-Ox-EY in vitro. Both conjugates selectively label EGFR in a light-dependent fashion, which is competed off by exogenous EGF. (**D**) EGFR is biotinylated by all three photo-probes: diazirine-biotin, aryl-azide-biotin, or phenol-biotin by using Ctx-EY. (**E**) Biotinylation sites of diazirine-biotin (yellow), aryl-azide-biotin (cyan), biocytin-hydrazide (purple), and phenol-biotin (maroon) highlighted on the crystal structure of the EGFR ECD (gray) in complex with Ctx Fab (blue) (PDB ID 1YY9; data taken from tables S5 to S8).

light-dependent manner (Fig. 2C), indicating that the conjugation of EY did not interfere with Ctx binding to EGFR as expected. Preincubation of EGF prevented labeling, demonstrating that direct binding is necessary for target labeling (Fig. 2C). To explore the generality of the workflow, we performed the same NHS and oxaziridine bioconjugation and labeling using a trastuzumab (Trz) Fab that binds the HER2 (human epidermal growth factor receptor 2) receptor ECD (fig. S4A) (*35*). Similar intermolecular labeling of HER2 was observed with Trz-NHS-EY or Trz-Ox-EY in a light-dependent manner. The demonstration of EGFR and HER2 labeling in vitro supports the broad applicability of the bioconjugation strategy and photo-probe labeling workflow.

We chose to focus on the NHS-azide conjugate (abbreviated to Ctx-EY) given its higher bioconjugation and photo-probe labeling efficiency. We evaluated the EGFR labeling efficiencies with diazirine-, aryl-azide-, and phenol-biotin photo-probes in parallel (Fig. 2D). All three probes labeled the EGFR ECD to increasing levels: aryl-azide-biotin > phenol-biotin > diazirine-biotin. The differing yields likely result from the combined effects of the reactive radical intermediates: half-lives (phenol ≫ aryl-azide > diazirine), yield of reaction with protein (phenol > aryl-azide > diazirine), and amino-acid preference observed (diazirine ~ aryl-azide ≫ phenol) (fig. S4B) (*36*–*38*).

We analyzed the specific sites of biotinylation for self-labeling of BSA and binary complex labeling of Ctx and EGFR with different photo-probes using mass spectrometry (MS) analysis (tables S1 to S8 and fig. S3, B and C). For diazirine-biotin, we found 17 biotinylated sites on BSA (table S1) and 30 sites on the Ctx-EGFR complex (table S5), with good coverage of modified peptides over the light and heavy chains of Ctx, as well as EGFR ECD (Fig. 2E and fig. S4C). We further characterized the modification sites on BSA and Ctx-EGFR systems for the other probes (tables S1 to S8 and fig. S4, B and C). As expected, phenol-biotin mostly labeled Tyr and Trp, whereas labeling with biocytin-hydrazide was found exclusively on His. Diazirine-biotin and aryl-azide-biotin showed very broad amino acid preference, which is consistent with previous reports (*20*, *37*).

Ctx-EY catalyzes targeted labeling of EGFR on cells

We next evaluated the ability of Ctx-EY to bind EGFR and label live cells (Fig. 3A). First, we incubated the Ctx-EY conjugate with an epithelial skin cancer cell line, A431 cells, that endogenously expresses very high levels of wild-type EGFR [normalized transcripts per million (nTPM) = 2978] (*39*, *40*). On-cell binding for the Ctx-conjugates, both Ctx-EY and Ctx-Ir, was confirmed with flow cytometry, showing that the conjugation of EY or the Ir-catalyst did not affect binding (Fig 3B). Detailed titration from 1 nM to 10 μM of Ctx and Ctx-EY analyzed with flow cytometry further confirmed that conjugation did not detectably affect cell binding (Fig. 3B and fig. S5A). We also tested A549 cells with more typical levels of EGFR (nTPM=59.7) (fig. S5B) (*41*) as well as NCI-H441 cells with very low EGFR expression (nTPM = 29.8) (fig. S5C), both of which showed proportionally

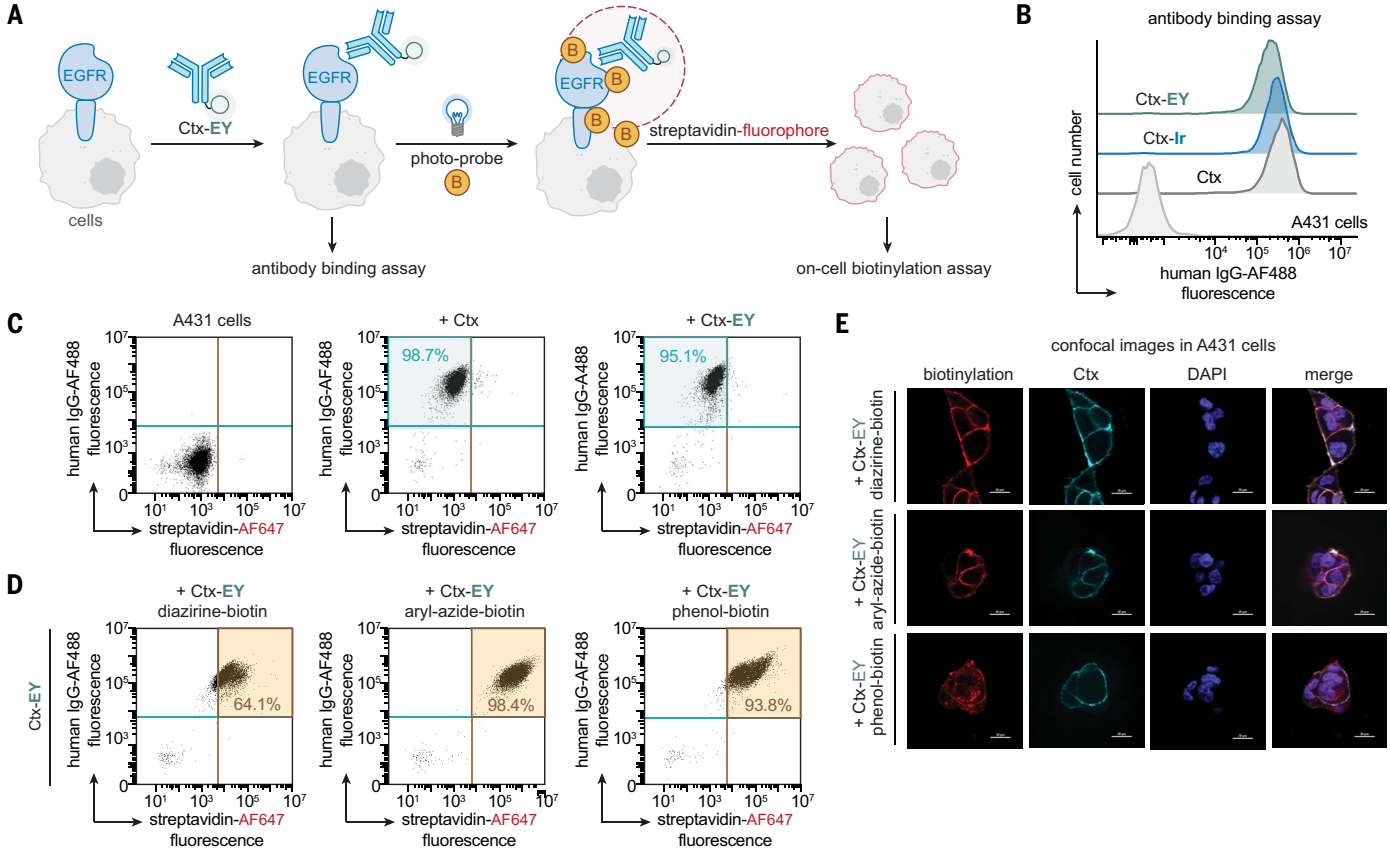

Fig. 3. Ctx-EY enables EGFR-dependent labeling on cells with different photo-probes. (**A**) General on-cell labeling workflow by using Ctx-EY conjugate and detection of biotin labeling by using streptavidin-fluorophore. (**B**) Cellular binding assay of 100 nM Ctx, Ctx-EY, or Ctx-Ir conjugates on A431 cells by means of flow cytometry analysis shows similar on-cell binding. (**C** and **D**) Quantitative on-cell (C) binding and (D) labeling with diazirine-biotin, aryl-azide-biotin, and phenol-biotin triggered by 100 nM Ctx-EY on A431 cells by means of flow cytometry analysis. (**E**) Confocal microscopy imaging of antibody binding and on-cell biotinylation of Ctx-EY on A431 cells shows labeling mostly confined to cell surface. Scale bar, 20 μm.

reduced binding of Ctx-EY and was similar to that of Ctx.

We next performed on-cell proximity labeling with diazirine-, aryl-azide-, and phenol-biotin photo-probes upon blue LED illumination (Fig. 3D and fig S6, A to E). We tested a range of Ctx-EY concentrations and observed efficient biotinylation on cells at 100 nM (Fig. 3D and fig. S6A). The diazirine-biotin, aryl-azide biotin, and phenol-biotin labeling caused a major shift of biotinylation in the flow cytometry profile of 64, 98, and 94%, respectively, in A431 cells (Fig. 3D). This is consistent with the order of labeling efficiencies observed in vitro. Similar patterns of biotinylation were observed in A549 and NCI-H441 cells (fig. S6, B and C), which were proportional to their EGFR expression levels (fig. S6D). Ctx-Ir only activated cell biotinylation with diazirine-biotin and aryl-azide-biotin and not phenol-biotin (fig. S6E).

We further visualized with confocal microscopy cell biotinylation induced by Ctx-EY (Fig. 3E and fig. S6, F and G). The labeled A431, A549, and NCI-H441 cells were costained with both α-human immunoglobulin G (IgG)–AlexFluor488 and streptavidin-AlexaFluor647 to visualize Ctx and biotinylation, respectively. We confirmed that the Ctx-EY conjugate was located on the cell membrane. Biotinylation by using the diazirine- and aryl-azide-biotin photo-probes was observed mainly on the cell membrane, whereas the phenol-biotin labeling was more diffuse, which is consistent with the longer half-life and labeling range of the phenoxyl radical.

We next developed a proteomics workflow to label the EGFR neighborhood (Fig 4A), focusing first on A431 cells with the highest levels of EGFR and using the most reactive diazirine-biotin photo-probe. We incubated A431 cells with or without EGF competition first and then performed the on-cell biotinylation workflow using Ctx-EY, followed by biotin enrichment using neutravidin beads. WB analysis confirmed selective biotinylation of EGFR, which was ablated in the presence of EGF (Fig. 4B). We also observed dose-dependent EGFR labeling over a wide range of Ctx-EY concentrations of 1 to 1000 nM, which was competed off by either EGF or unlabeled Ctx (fig. S7A).

Cells were treated with Ctx-EY in the presence or absence of EGF competition, and biotinylated proteins were captured on neutravidin beads and digested on-bead with trypsin. Samples were prepared in biological triplicate for MS analysis by using label-free quantitation (Fig. 4C, volcano plot, and fig. S7B, heatmap). We identified a total of 536 proteins with 41 proteins enriched by more than two-fold with Ctx-EY relative to EGF competition [$\log_2$(ratio) ≥ 1, $P < 0.05$, unique peptide ≥ 2] (table S9 and fig. S7, C and D). EGFR was among the highly enriched as expected. Gene Ontology (GO) analysis showed representation of biological processes that include regulation of phosphatase activity as well as molecular function entities such as phosphatase activator activity (fig. S7D). These features are consistent with the functional roles of EGFR signaling and suggest that the enriched EGFR interactors are accurately represented.

We orthogonally confirmed with biotin-immunoprecipitation (biotin-IP) that six top hits were biotinylated, in which streptavidin pull-down samples were analyzed by means of WB by using specific antibodies after proximity labeling (Fig. 4D). Among them, five were observed to coimmunoprecipitate with EGFR (Fig. 4D). All six proteins are known to either

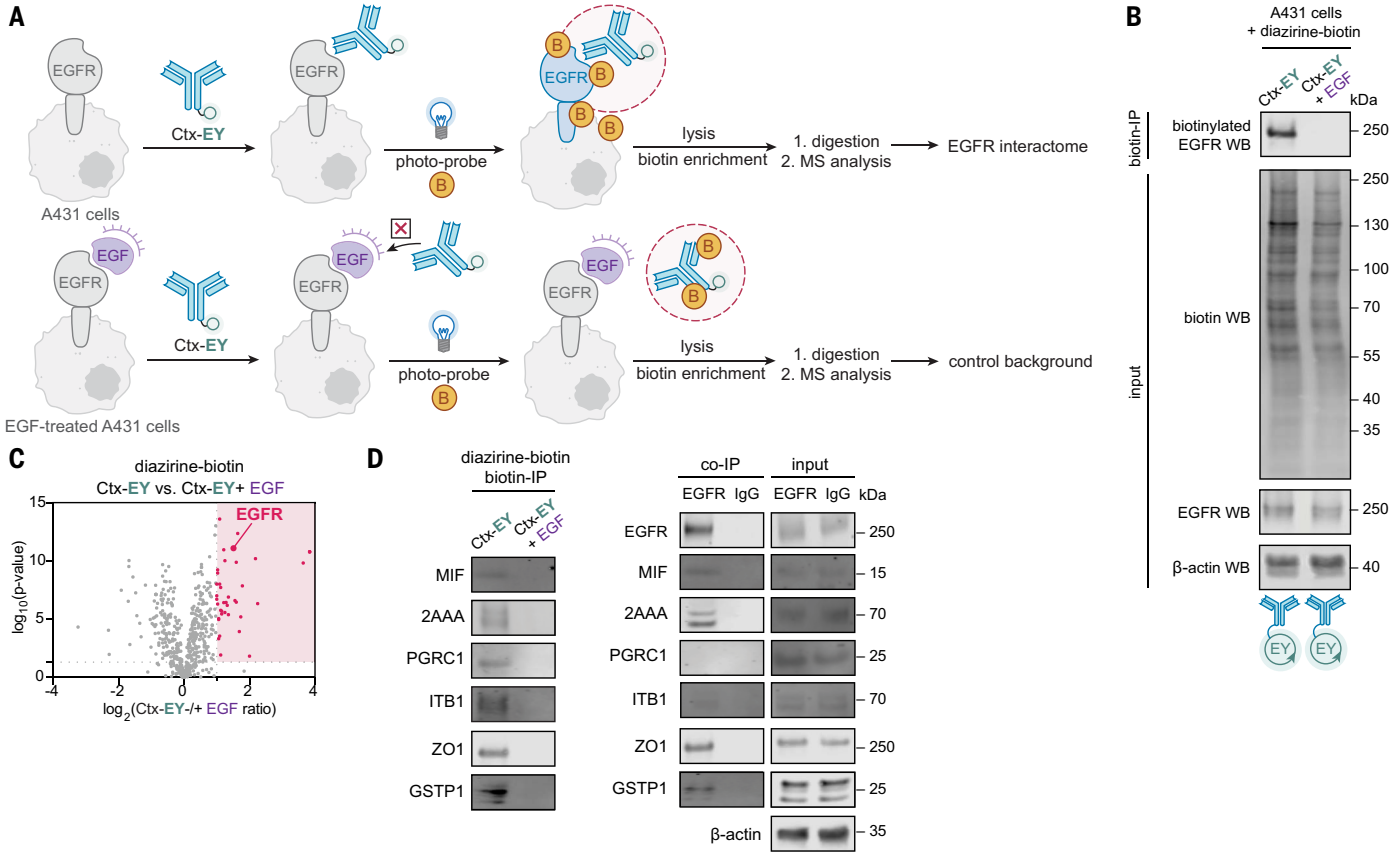

Fig. 4. High-resolution profiling of the EGFR neighborhood by using MultiMap. (**A**) General proteomics workflow of interactome profiling by using Ctx-EY conjugate with or without EGF competition. (**B**) WB showing biotinylation with the diazirine-biotin photo-probe on A431 cells by using Ctx-EY in the absence and presence of EGF competition. (**C**) Volcano plot of Ctx-EY–mediated labeling of EGFR with or without EGF on A431 cells by using diazirine-biotin. Forty-one significantly enriched proteins [$\log_2$(ratio) ≥ 1, $P < 0.05$, unique peptide ≥ 2, $n = 3$] are highlighted in red and listed in table S9. (**D**) Validation of six top protein hits by using biotin-IP blots. Five were selectively enriched in a separate EGFR co-IP experiment. Full heatmap is presented in fig. S8B and table S9.

functionally interact with EGFR or were found in immunoprecipitation experiments (*42*–*44*). These include integrin beta 1 (ITB1), which is critical for stable maintenance for EGFR on the cell membrane (*45*, *46*), as well as macrophage migration inhibitory factor (MIF), an immunostimulatory cytokine regulated by matrix metalloproteinase 13 (MMP13), which is known to be inhibitory for EGFR activation (*47*). Others include substrates of EGFR such as glutathione *S*-transferase P1 GSTP1 (*48*) and tight junction protein ZO1 (*49*), both of which are known to be activated upon phosphorylation by EGFR. One target membrane-associated progesterone receptor component 1, PGRC1, was not observed in EGFR coimmunoprecipitatation (co-IP) experiments, and we would expect that some interactions may not be strong enough to survive the co-IP workup in these cells.

Multiscale EGFR interactome profiled with MultiMap

Having demonstrated that the proteomic workflow of Ctx-EY triggered biotinylation on cells expressing high levels of EGFR, we expanded to cells expressing modest levels of EGFR. Lung cancer cell line A549, for example, expresses lower amounts of EGFR (nTPM = 59.7), which is more typical of native membrane proteins (*41*). We applied all photo-probes, and EGFR was selectively biotinylated with each probe (fig. S8A). Applying the proteomics workflow, we then identified EGFR neighbors enriched with diazirine-biotin, aryl-azide-biotin, and phenol-biotin by comparing labeling with Ctx-EY in the absence and presence of EGF (Fig. 5A). We found that EGFR is one of the most enriched proteins from all three datasets (tables S10 to S12). Enriched proteins were identified with the same statistical thresholds [$\log_2$(ratio) ≥ 1, $P < 0.05$, unique peptide ≥ 2, $n = 3$], which allowed us to compare protein identities across reactions with different photo-probes. We identified 72 proteins using diazirine-biotin, 188 using aryl-azide-biotin, and 188 using phenol-biotin (tables S10 to S12 and fig. S8, B to D).

As represented in a Venn diagram (Fig. 5B), there were a total of 322 different proteins enriched over the controls in at least one of the three photo-probes. Aryl-azide-biotin and phenol-biotin labeled more proteins than did diazirine-biotin, reflecting the formers' higher yields and relatively long labeling radii. We found that >80% of the enriched proteins were annotated in UniProt as plasma membrane proteins [plasma membrane; Gene Ontology (GO) ID 0005886] for all three photo-probes. GO enrichment analysis suggested that molecular functions such as EGFR activity and EGF binding were highly enriched (fig. S8D).

Sixteen candidate neighbors were identified in all three datasets of MultiMap (Fig. 5B). Although no direct structural evidence has been reported for EGFR with any of these proteins, CD44 and Galectin-3 have been functionally associated with EGFR: CD44 regulates EGFR functions in the presence of CD147 and hyaluronan (*50*, *51*); Galectin-3 regulates EGFR localization, and its interactions have been suggested through genetic studies in pancreatic cancers (*52*). Both targets were further validated by means of biotin-IP and EGFR co-IP (Fig. 5C), supporting that they are proximal neighbors of EGFR.

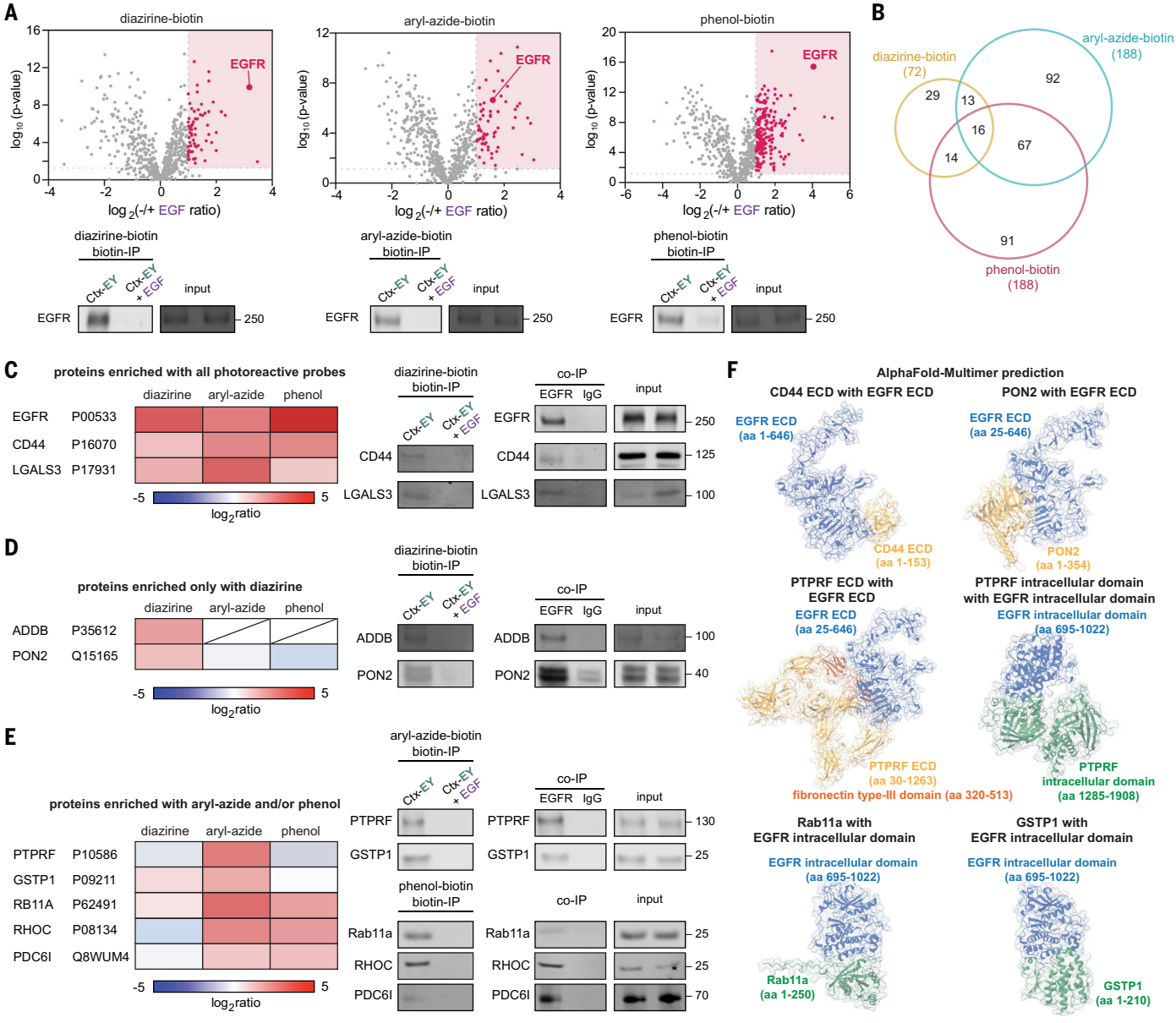

Fig. 5. MultiMap reveals a multiscale EGFR interactome network. (**A**) Volcano plots of Ctx-EY–mediated EGFR interactome profiling on A549 cells by using three different photo-probes (biotin-diazirine, aryl-azide-biotin, or phenol-biotin, respectively). Significantly enriched proteins [$\log_2$(ratio) ≥ 1, $P < 0.05$, unique peptide ≥ 2, $n = 3$] are highlighted in red and listed in tables S10 to S12. (**B**) Venn diagram of EGFR interactome enriched from A431 cells by using different photo-probes. (**C**) Enrichment ratios and validation of protein hits by using all three photo-probes. (**D**) Enrichment ratios and validation of protein hits from only the diazirine-biotin dataset. (**E**) Enrichment ratios and validation of protein hits from both aryl-azide-biotin and/or phenol-biotin datasets. (**F**) AlphaFold-Multimer predictions of EGFR complexes confirmed the direct interactions of EGFR with interactors found with MultiMap. EGFR ECD or ICD (blue) is shown in complex with the corresponding interactor protein (yellow for the ones interacting with EGFR ECD, green for the ones interacting with EGFR ICD) along with the pDockQ scores and BSASA.

We next expanded our list to the 29 proteins that were in common for diazirine-biotin and aryl-azide-biotin, the photo-probes with high labeling resolutions (Fig. 5D and fig. S8E). Among them, we found a paraoxonase, PON2, as well as two proteins associated with RTK phosphorylation and activation: β-adducin ADDB and mitogen-activated protein kinase pathway member BRAF (serine/threonine-protein kinase B-raf) (*53*, *54*). Both PON2 and ADDB were detected with biotin-IP and EGFR co-IP. BRAF, a cytosolic protein, was enriched by biotin-IP but not EGFR co-IP, suggesting that it is close but may not be in physical contact. Between the diazirine and aryl-azide datasets, we identified the known EGFR functional interactors such as Tid1 (*55*) and ITB1 also found in the A431 cell experiments, as well as previously unreported interaction partners, including CKAP4 and RAC1.

The aryl-azide-biotin and phenol-biotin experiments contributed more proteins (293 in total). Among the top hits were the tyrosine-protein phosphatase receptor PTPRF, glutathione transferase GSTP1, small guanosine triphosphatase (GTPase) Rab11a, Rho-related guanosine 5′-triphosphate (GTP)–binding protein RHOC (ras homolog family member C), and ESCRT (endosomal sorting complexes required for transport) protein PDC6I (programmed cell death 6-interacting protein) (Fig. 5E and fig. S8E). All were detected with biotin-IP, with 10 out of 11 of these proteins coimmunoprecipitated

with EGFR, suggesting that they form relatively stable complexes.

To provide a structural level of analysis, we turned to AlphaFold-Multimer, an extension of AlphaFold developed over the past few years that uses artificial intelligence to generate plausible models of binary protein complexes (*25*, *56*, *57*). This community has developed scoring metrics such a predicted DockQ score (pDockQ), in which a threshold of >0.23 retrieves 51% of true-positive interacting proteins with a false-positive rate of ~1% in large test set models (*58*). Additional criteria can be applied, including buried solvent accessible surface area (BSASA) ≥ 500 Å^2 (*59*, *60*), predicted local distance difference test (pLDDT) > 50 for the interface residues, and minimum predicted alignment error (PAE) < 15 Å, as described previously (*56*). As a true-positive example, we derived an AlphaFold-Multimer model of the EGF:EGFR complex (fig. S9A and table S13) that closely overlaid that of the known structure of EGF:EGFR (PDB ID 1IVO; root mean square deviation between 469 atom pairs is 0.924 Å) (*61*).

We applied AlphaFold-Multimer to candidate neighbors validated by means of biotin-IP and/or EGFR co-IP in A431 and A549 cells and generated a total of 29 models. As shown in waterfall plots, the average pDockQ score (0.298) and BSASA (1466Å^2) for the 29 EGFR-protein pairs were both above the established criteria, suggesting direct interactions (fig. S9B and table S13). We next applied AlphaFold-Multimer to compute models of all potential heterodimeric complexes from Figs. 4C and 5A (table S13). To increase the accuracy of the models for transmembrane proteins (*62*), we calculated separately the ECD (amino acids 1 to 646) and intracellular domain (ICD; amino acids 695 to 1022) of EGFR and paired them with the corresponding ECDs or ICDs of transmembrane protein targets. As previously described, we retained only high-confidence AlphaFold-Multimer models (average pLDDT > 50, minimum PAE < 15 Å) (*56*) and performed further filtering using the aforementioned criteria (pDockQ score ≥ 0.23, BSASA ≥ 500 Å^2). The final list of validated complexes included the binary complexes of EGFR ECD with CD44 ECD (amino acids 1 to 153, pDockQ = 0.375), PON2 (pDockQ = 0.372), and MIF (amino acids 1 to 115, pDockQ = 0.375) (Fig. 5F and fig. S9, C to F). In addition, the ICD of EGFR is predicted to bind Rab11a (pDockQ = 0.264), GSTP1 (pDockQ = 0.535), and RAC1 (pDockQ = 0.387) (Fig. 5F and fig. S10, A to C). One of the AlphaFold-Multimer complexes predicted with the highest confidence is a cell-surface phosphatase, PTPRF, where PTPRF ECD binds EGFR ECD (pDockQ = 0.429), and likewise, the PTPRF ICD binds the EGFR ICD (pDockQ = 0.476) (Fig. 5F, bottom).

MultiMap can capture distal synaptic protein networks

Extracellular protein-protein interactions occur not only in cis on the cell membrane but also in trans between cell-cell junctions. To explore PLP of cell synapses by using MultiMap at different labeling radii, we assembled a coculture system in which the cell-cell interaction was induced by a bispecific T cell engager (BiTE) (Fig. 6A). This BiTE contained the Ctx Fab genetically fused to an α-CD3 scFv (OKT3) (*63*). We used two different cells in the coculture system: a human embryonic kidney (HEK) 293T cell engineered to overexpress a Flag-tagged-EGFR (HEK-Flag-EGFR) and well-established Jurkat cells expressing a nuclear factor of activated T cells (NFAT)–green fluorescent protein (GFP) reporter (*64*). In this design, the Flag tag served as an orthogonal ecto-epitope for an EY-conjugated α-Flag antibody (α-Flag-EY), allowing an alternative strategy of ecto-epitope–based selective recognition apart from direct antibody recognition in our EGFR studies. To separately characterize the labeling on HEK-Flag-EGFR and Jurkat NFAT-GFP cells, we used α-CD3-PE signal to allow facile separation of CD3$^+$ Jurkat cells from CD3$^-$ HEK-Flag-EGFR by means of fluorescence-activated cell sorting (FACS). Levels of cis- and trans-labeling from α-Flag-EY were determined with flow cytometry. Proteins labeled with different photo-probes were enriched by using streptavidin beads and analyzed by means of WB (Fig. 6A).

We first monitored BiTE engagement between HEK-Flag-EGFR and Jurkat NFAT-GFP cells using the standard GFP reporter readout. As expected, we observed dose-dependent BiTE activation of cell-cell engagement, with the 80.3% shift of GFP signal in the presence of 8 nM EGFR BiTE and 92.3% with 50 nM BiTE (fig. S11A). The GFP expression was not affected by the presence of α-Flag-EY, indicating that the Flag ecto-epitope recognition did not interfere with the cell-synapse engagement. We then performed the MultiMap workflow using four photo-probes of increasing labeling range: diazirine-biotin, aryl-azide-biotin, biocytin-hydrazide, and phenol-biotin. We monitored biotinylation in cis for HEK-Flag-EGFR and in trans for Jurkat NFAT-GFP using a streptavidin-AlexaFluor647 signal (Fig. 6A and fig. S11, B and C). Cis-labeling of HEK-Flag-EGFR cells occurred for >60% of cells for the diazirin-biotin, aryl-azide-biotin, and phenol-biotin, with ~29% for the biocytin hydrazide (fig. S11B). By contrast, in cells overexpressing EGFR without the Flag tag, minimal shift (~3 to 4%) was observed on these controls, suggesting that biotinylation induced by α-Flag-EY is highly selective. The trans-labeling of the Jurkat cells by using the shorter-range diazirine-biotin, aryl-azide-biotin was limited to 3 to 4% (fig. S10C), whereas the intermediate-range biocytin-hydrazide and long-range phenol-biotin labeled 9 and 22%, respectively (Fig. 6A and fig. S11C). This is consistent with the cell-cell synapse distance based on the length of the Fab-ScFv BiTE (*65*), plus the sizes of the EGFR ECD and the CD3 complex. By further analysis with WB, the cis-target EGFR was observed by means of biotin-IP enriched in the presence of the three photo-probes, whereas trans-target CD3 was primarily enriched in the phenol-biotin sample, with moderate amount observed in the aryl-azide-biotin–labeled sample (Fig. 6A). Thus, longer-range photo-probes are more efficient for trans-labeling, which is consistent with previous studies (*24*).

To further expand the generality of MultiMap for cell-cell synapses, we tested the BiTE system to two other cancer targets, HER2 and CUB domain containing protein 1 (CDCP1) (Fig. 6B and figs. S12 and S13). We fused α-HER2 Fab sequence (Trz Fab) and a previously generated α-CDCP1 Fab (4A06) (*63*) onto the CD3 scFv scaffold (Fig. 6B and fig. S12A). Again, we observed dose-dependent cell-cell engagement in the presence of both engineered BiTEs and antigen-expressing cells as well as a similar biotinylation pattern (figs. S12, B and C, and S13, A and B): cis-labeling was found with all three photo-probes, and trans-labeling activated primarily with phenol-biotin. By introducing EY directly on the BiTE construct, we further performed confocal imaging in the HEK-Flag-CDCP1/Jurkat NFAT-GFP coculture system and confirmed that biotinylation primary occurred at the cell-cell synapse (fig. S13C).

To examine the proteins at the cell synapse, we first separated HEK293T-CDCP1 and Jurkat-NFAT-GFP cells using FACS and enriched biotinylated proteins from either cell. In particular, we confirmed selective biotinylation of CDCP1 with all three photo-probes and CD3 with only phenol-biotin (Fig. 6B). We quantitatively profiled the proteins captured at either side of the cell synapse between HEK-Flag-CDCP1 and Jurkat NFAT-GFP (Fig. 6C and table S14). We discovered that CDCP1 was enriched in the cis-labeled samples. Proteins from the CD3 complex, including CD3δ and CD3ε, were highly enriched in the trans-labeled samples. Similarly, CDCP1 and CD3 components were also selectively enriched in BiTE-EY–labeled samples when compared with an IgG isotype control (fig. S13D and table S15). Additional CDCP1 epitope-free control using wild-type HEK293T confirmed that the selective protein enrichment is epitope dependent (fig. S13D and table S16). These results demonstrate that the MultiMap workflow can selectively label proteins at the BiTE-induced cell-cell synapse.

Last, we evaluated MultiMap labeling at a (CAR)T cell–cell synapse (Fig. 6D and fig. S14). Jurkat cells expressing a Myc-tagged CAR construct (Jurkat-CAR) that targets CD19 were

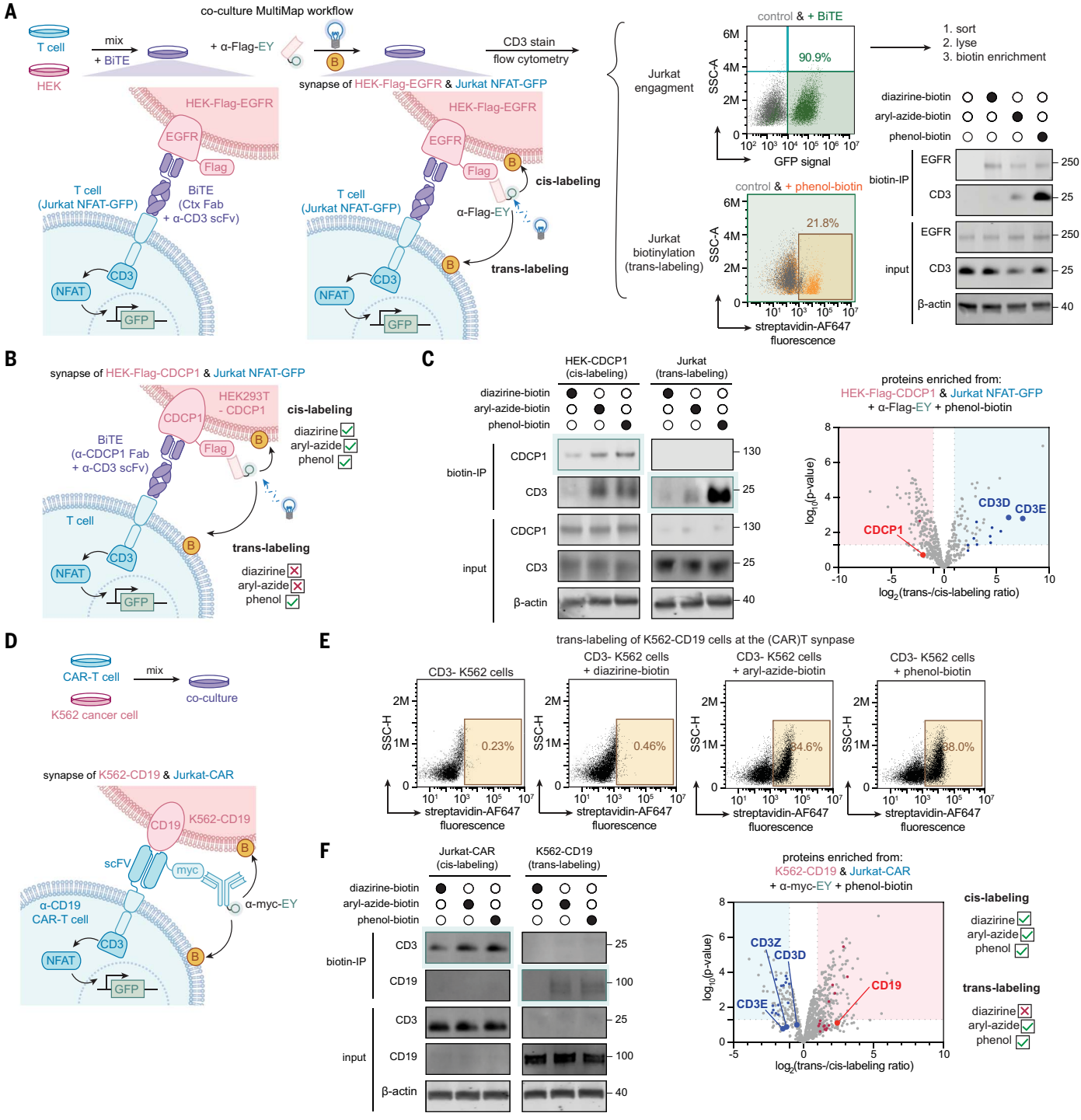

Fig. 6. MultiMap enables targeted snapshots of local cell-cell synapses. (**A**) On-cell labeling of the T cell synapse by using a BiTE that recognizes EGFR. Jurkat NFAT-GFP and HEK293T-Flag-EGFR were co-cultured in the presence of the BiTE before MultiMap was performed by using an EY-conjugated α-Flag nanobody (α-Flag-EY). Cell-cell engagement was monitored by means of NFAT-GFP reporter gene activation. Photocatalytic labeling was characterized by means of flow cytometry before biotin-enriched proteins were analyzed with WB. Full flow data are shown in fig. S11. (**B**) Target biotinylation of CDCP1 and CD3 at the T cell synapse by using a BiTE that recognizes CDCP1. Longer labeling radius by using phenol-biotin was necessary for trans-labeling on Jurkat NFAT-GFP. (**C**) Volcano plot of proteins biotinylated on HEK-Flag-CDCP1 (cis-labeling) and Jurkat NFAT-GFP (trans-labeling) by using phenol-biotin. Significantly enriched proteins from HEK-Flag-CDCP1 [$\log_2(\text{ratio}) \leq -1$, $P < 0.05$, unique peptide ≥ 2, $n = 3$] or Jurkat NFAT-GFP [$\log_2(\text{ratio}) \geq 1$, $P < 0.05$, unique peptide ≥ 2, $n = 3$] are shaded in blue and red, respectively. Proteins known to associate with CDCP1 in Search Tool for the Retrieval of Interacting Genes/Proteins (STRING) analysis are highlighted in red, and those associated with CD3 complex are highlighted in blue. Full protein lists are shown in table S14. (**D**) Scheme of on-cell labeling of α-CD19 (CAR)T cell system. (**E**) (CAR) T cell–mediated trans-labeling of K562 cancer cells by using all photo-probes. (**F**) (Left) Target biotinylation of CD3 and CD19 at the CAR-T synapses by use of WB and MS analyses. Cells were sorted to differentiate cis- and trans-labeling before

biotinylated proteins were enriched for analysis. Both phenol-biotin and aryl-azide-biotin enabled trans-labeling. (Right) Volcano plot of proteins biotinylated on Jurkat-CAR (cis-labeling) and K562-CD19 (trans-labeling) by using phenol-biotin. Significantly enriched proteins from Jurkat-CAR [$\log_2$(ratio) ≤ −1, P < 0.05, unique peptide ≥ 2, n = 3] or K562-CD19 [$\log_2$(ratio) ≥ 1, P < 0.05, unique peptide ≥ 2, n = 3] are shaded in blue and red, respectively. Proteins known to associate with the CAR complex in STRING analysis are highlighted in blue, and those associated with CD19 are highlighted in red. Full protein lists are shown in table S17.

mixed with K562 cancer cells expressing CD19 ectodomain (K562-CD19). With an EY-conjugated α-myc antibody (α-myc-EY), we performed our workflow by introducing cis-labeling on K562-CD19 and trans-labeling on Jurkat-CAR cells. We confirmed cell engagement by monitoring the CAR activation with or without K562 cells (fig. S14A). We observed cis-labeling on interacting CAR cells with all photo-probes (fig. S14B). The longer-range photo-probes, aryl-azide-biotin and phenol-biotin achieved trans-labeling, with a much lower level of biotinylation by using the short-range diazirine-biotin (Fig. 6E). The same results were confirmed with WB analysis (Fig. 6F). These results are in line with the estimate of cell-cell distance between CAR-induced synapse at ~120 Å according to AlphaFold prediction (*66*), which is shorter than BiTE-induced synapse. We then sorted each cell type for proteomics analysis and found that both CD19 and CD3 component enriched for trans-labeling and cis-labeling (Fig. 6F and table S17). Direct comparison of labeled proteins at the CAR-T synapse with the isotype and CD19-epitope–free controls further confirmed the selectivity in synaptic labeling (fig. S14C and tables S18 and S19). Taken together, our data suggest that MultiMap can label cells at the cell-cell synapses and map the proteins in proximity. Only minimal alternation to the existing workflow is needed for labeling in different cell-cell engagement scenaios. Looking forward, we anticipate that this platform will be a useful technology to identify key proteins in different synaptic environments.

Discussion

We have demonstrated a multiscale PLP technology, MultiMap, that enables proximity labeling and interactome profiling with adjustable resolution. The photocatalyst EY is capable of triggering a broad range of photo-probes with different half-lives. It is commercially available, biocompatible, and shown to be readily conjugated to seven different proteins and antibodies by use of commonly accessible methods. Simple targeting by EY-conjugated antibodies obviates the need for cell engineering. EY-mediated labeling is rapid and light-dependent, which potentially allows kinetic control of the labeling. Future structure-activity relationship studies on EY, as done for rhodamine- or fluorescein-based scaffolds (*67*), could enhance our understanding of the photochemical mechanisms of EY-triggered labeling (*6*, *68*) as well as improve its spectral properties, activation efficiency, and use in tissues (*18*, *21*, *28*).

Coupled with standard biochemical validation and the recently developed AlphaFold-Multimer algorithm for structural prediction (*25*), the MultiMap PLP workflow provides three orthogonal and integrated pillars for high-resolution profiling of protein neighborhoods. In addition to identification of new potential neighbors, we detected many proteins known to functionally interact with EGFR that are reported to stabilize, modulate, or act as substrates for EGFR. One of the most striking targets identified was the phosphatase PTPRF, which could be a functional off-switch for EGFR. AlphaFold-Multimer predicts that the ECD of PTPRF binds to the back side of the EGFR ECD away from the dimer interface and that the ICD of the phosphatase binds to the intracellular kinase domain of EGFR. Despite that antibodies to EY recognize extracellular targets, we found that some of the high-confidence hits were intracellular proteins. Some are known to functionally associate with EGFR, for which high-confidence AlphaFold-Multimer binary models were constructed. It is possible that the labeling is caused by cell penetrance of the activated photo-probe when triggered by EY. We believe future work could fine-tune the properties of photo-probes such as charge and hydrophobicity to achieve extracellular-only or organelle-specific labeling.

It is unlikely that all these identified neighbors bind simultaneously to EGFR. Some proteins are predicted to bind over the same sites. These data suggest that EGFR can be in multiple neighborhoods that are dynamic and may have multiple functions that are yet to be revealed. The binder we used in this study, Ctx, is an inhibitor of EGFR function. Thus, candidates identified in our studies are specifically from the EGFR off-state neighborhood. We envision that MultiMap will be useful to study on-state, drug-bound, and resistance-mutant neighborhoods, which will give a comprehensive map of the EGFR interactomes. Founding studies of growth factor signaling emphasized linear protein-protein interactions from outside to inside. Identification of cell surface interactomes indicates that signaling may be promoted in a horizontal manner by lateral protein-protein complexes.

MultiMap was also effective for long-range labeling of cell-cell synapses. As shown for the ones activated by BiTE or (CAR)T, we found that spatial variability among synaptic junctions can be addressed by using photo-probes with different labeling radii. The advantage of MultiMap allowing multiscale labeling potentiates its application for interactome profiling of additional intercellular interaction networks. Information of these networks will help to deepen our understanding of the underlying mechanisms behind intercellular recognition and signaling. In cases in which antibodies are not available, one can use a genetically encoded ecto-tag on the target ECD, similar to the Flag and myc ecto-tags we introduced in our study. We can also envision proteome-wide interactome profiling for membrane proteins by using these ecto-tags on par with the scale for the intracellular OpenCell system (*69*).

We recognize that despite the confidence and accelerated process in target identification with MultiMap, information on candidate neighborhoods warrants further confirmation through more in-depth structural, mutational, and functional studies. Nonetheless, we believe that MultiMap PLP integrated with in silico prediction can begin to provide plausible models for binary protein interactions with high structural precision. This would be a crucial step forward to begin to construct a structural map of the protein-protein interactome on the cell surface. In addition, understanding how the surfaceome functions in concert with the external environment communication may suggest new neocomplexes to target for both small molecules and biologics.

Materials and methods

General methods and instrumentation

Illumination was performed using a Penn PhD Photoreactor M2 (Sigma Aldrich, Z744035) with a 450 nm blue light source module (Sigma Aldrich, Z744033) at 100% intensity, or LED array light sources (Thor Labs, LIU470A for 470 nm LED array, LIU525B for 525 nm LED array) along with a LED mounting adapter (AD38). To use Penn PhD Photoreactor, fan speed was set at 6800 rpm under manual control with 100/min stirring and samples were illuminated at 100% intensity for indicated time. To use LED array light sources, samples were placed under a Thor Labs LED array light source, which provides 4.0 mW/cm^2 (470 nm) and 1.9 mW/cm^2 (525 nm) intensity at 100 mm distance from the LED according to information from the manufacturer. Flow cytometry experiments were performed on a CytoFlex flow cytometer (Beckman CytoFlex) and analyzed using FlowJo software. Cell sorting experiments were performed on a SONY cell sorter (SONY, SH800). Proteomics experiments were performed on a TimsTOF PRO (Bruker) equipped with a CaptiveSpray source and a nanoElute System. The peptides were separated on a 25 cm, ReproSil c18 1.5 μM 100 Å column (PepSep,

PN # PSC-25-150-15-UHP-nc). Protein quantification was performed by bicinchoninic acid assay on a multimode microplate reader Infinite 200 PRO (Tecan Trading AG, Switzerland). Sonication of cells or protein pellets was performed using a QSonica Q500 Sonicator (QSonica Sonicators, Newtown, CT). DNA, RNA or protein concentrations were measured using a NanoDrop 2000 spectrophotometer (Thermo Scientific).

For immunoblotting analysis, proteins were loaded on 4–12% BisTris gels (Bolt 4–12% 17-well, Thermo Fischer, NW04127BOX), and transferred from SDS-PAGE gels to PVDF membranes (Thermo Fischer, IB24002) using an iBlot-2 dry blotting system (Thermo Scientific, IB21001). Membranes were blocked with Tris buffered saline (TBST, 37mM sodium chloride, 20mM Tris, 2.7mM potassium chloride, 0.05% Tween 20; pH = 7.4) containing 0.1% Tween-20 and 5% BSA and incubated with the primary antibodies and the secondary antibodies sequentially including anti-rabbit IgG Goat IR800 secondary antibody (Rockland, 926-32211), anti-rabbit IgG Goat IR680 secondary antibody (Rockland, 611-144-002), anti-rabbit IgG Goat secondary antibody peroxidase (Rockland, 611-1302), anti-mouse IgG Goat IR800 secondary antibody (Rockland, 610-145-211), and anti-mouse IgG Goat IR680 secondary antibody (Rockland, 610-144-002). Immunoblots images were captured by an infrared LI-COR imager (Odyssey CLx). In-gel fluorescence and immunoblot fluorescence signals were detected on a BioRad imager (ChemiDoc XRS+ System).

General chemical reagents and instrumentation

Chemicals were purchased including TFPA-PEG_3-biotin (Thermo Scientific, 21303), biotinyl tyramide (Sigma-Aldrich, SML2135), eosin-5-isothiocyanate (Biotium, 90091), 5-iodoacetamidoerythrosin (Alfa Chemistry, ALP3853), erythrosine B disodium salt (Alfa Aesar, A14180-14), DBCO-PEG_4-amine (Click Chemistry Tools, A103P-100; separately synthesized by ChemPartner), 2-(Prop-2-yn-1-yloxy)-4-(3-(trifluoromethyl)-3H-diazirin-3-yl)benzoic acid (Sigma-Aldrich, 900858), Eosin Y (Sigma-Aldrich, E4009), and Rose Bengal (Sigma-Aldrich, 33000). All solvents and reagents were purchased from chemical suppliers (Sigma Aldrich, Acros Organics, Thermo Scientific or VWR Chemicals BDH®) and were used as received unless otherwise noted. Flash Column Chromatography was performed using Teledyne ISCO CombiFlash EZ Prep chromatography system, employing pre-packed silica gel Teledyne ISCO RediSep cartridges. Protein mass spectra were obtained using a Waters Xevo G2-XS time-of-flight mass spectrometer operating with Waters MassLynx software (version 4.2). DBCO-PEG_3-EY was synthesized and characterized as shown in Scheme S1 (ChemPartner). Diazirine-biotin (diazirine-PEG_3-biotin) was synthesized and characterized according to published reports (*15*) (Medicilon).

Proton nuclear magnetic resonance spectrum (^{1}H NMR) and carbon nuclear magnetic resonance spectrum (^{13}C NMR) were recorded on a Bruker 400 MHz instrument at 25°C. Chemical shifts were reported in parts per million (ppm, δ scale) relative to residual solvent as an internal reference (DMSO: 2.50 ppm for ^{1}H and 39.52 ppm for ^{13}C). Data are represented as follows: chemical shift, multiplicity (s = singlet, d = doublet, t = triplet, q = quartet, quin = quintet, m = multiplet and/or multiple resonances, br = broad, app = apparent), integration, coupling constant (*J*) in Hertz (Hz), and assignment. Infrared (IR) spectrum was recorded on a Bruker ALPHA FT-IR and are reported in terms of frequency of absorption (cm^{-1}) and intensity of absorption (s = strong, m = medium, w = weak, br = broad).

Antibodies and biological reagents

Antibodies were purchased including: Ctx (cetuximab, Selleck Chemicals, A2000), Trz (trastuzumab, Selleck Chemicals, A2007), anti-EGFR (Thermo Scientific, MA5-13319; Cell Signaling Technology, 4267S), anti-HER2 (Cell Signaling Technology, 2165S), anti-MIF (Proteintech, 20415-1-AP), anti-GSTP1 (Proteintech, 15902-1-AP), anti-ZO1 (Proteintech, 21772-1-AP), anti-PGRMC1 (Cell Signaling Technology, 13856T), anti-Integrin β1 (Cell Signaling Technology, 4706S), anti-β-actin (Santa Cruz Biotechnology, sc-47778), anti-LGALS3 (Cell Signaling Technology, 12733S), anti-CD44 (Cell Signaling Technology, 3578S), anti-ADDB (Proteintech, 14640-1-AP), anti-PON2 (Abcam, ab183710), anti-PTPRF (anti-LAR, R&D system, MAB3004-SP; Cell Signaling Technology, 61611S), anti-Rab11a (Cell Signaling Technology, 2413S), anti-RHOC (Cell Signaling Technology, 3430T), anti-PDCD6IP (Proteintech, 12422-1-AP), anti-BRAF (Cell Signaling Technology, 14814S), anti-Tid1 (Cell Signaling Technology, 4775S), anti-CKAP4 (Proteintech, 16686-1-AP), anti-Rac1/2/3 (Cell Signaling Technology, 2465T), anti-DOCK4 (Proteintech, 21861-1-AP), anti-SIGMAR1 (Proteintech, 15168-1-AP), anti-PKACa (Cell Signaling Technology, 4782S), anti-DNAJC13 (Bethyl Laboratories, A304-872A), anti-β-catenin (Cell Signaling Technology, 8480T), anti-Flot2 (anti-Flotilin 2, Cell Signaling Technology, 3436S), mouse IgG1 isotype control (BD Biosciences, 556648), anti-CD3D (Cell Signaling Technology, 31857S; 85061S), anti-CD19 (Cell Signaling Technology, 90176T), anti-CDCP1 (Cell Signaling Technology, 4115S), and anti-Myc (Santa Cruz Biotechnology, sc-40). Anti-M1-FLAG antibody was purified in HEK293T cells using the sequence gifted by the Kruse lab (Harvard Medical School).

The following antibodies were used in flow cytometry assays: anti-CD3-AlexaFluor561 (Thermo Scientific, 505-0038-41), anti-CD3-PE (BioLegend, 300456), anti-CD19-PE (BioLegend, 302254), streptavidin-AlexaFluor488 (Thermo Scientific, S32354), streptavidin-AlexaFluor647 (BioLegend, 405237), anti-EGFR-AlexaFluor647 (Fisher Scientific, 352918), anti-human IgG-AlexaFluor488 (BioTechne, FAB110G), and anti-human IgG-AlexaFluor647 (BioTechne, FAB110R). Recombinant proteins included human EGFR (Bio-Techne, 1095-ER-002) and human HER2 (Acro Biosystems, HE2-H5225). Gels were imaged with InstantBlue protein stain (Expedeon, ISB1L). Albumin was purchased from Sigma-Aldrich (A1887). For enrichment assays, NeutrAvidin agarose beads (Pierce, 29200) and protein A magnetic beads (Cell Signaling Technology, 73778) were used. Cell lysis buffer was prepared by diluting from 10X cell lysis buffer (Cell Signaling Technology, 9803S) or from 10X RIPA buffer (EMD Millipore, 20-188). Sample loading buffer were diluted from 4X LDS sample loading buffer (G Biosciences, 786-323). Sequencing-grade modified trypsin (Promega, V5111), sequencing-grade chymotrypsin (Promega, V1061) and mini Bio-Spin columns (Bio-Rad, 7326207) were purchased. When performing solvent exchange processes, 7 kDa Zeba Spin desalting columns (Thermo Fischer, 89883) were used.

Plasmid construction

Plasmids for the Ctx-OKT3 BiTE, Trz-OKT3 BiTE, and α-CDCP1-OKT3 BiTE that targeted EGFR, HER2 and CDCP1, respectively were constructed by standard molecular biology methods and as previously described (*63*). For example, DNA fragments of Ctx Fab heavy and light chain were synthesized by integrated DNA technologies (IDT). OKT3 scFv was amplified using primers shown below. All BiTEs were constructed in the pFUSE-hIgG1 vector (InvivoGen) with IL-2 signal peptide for mammalian expression. Ctx Fab heavy chain was cloned on one vector, and the Fab light chain genetically fused with the N-terminus of OKT3 was cloned on a separate copy of the vector. The sequence of the linker between the light chain and scFv is as follows: GGGGS. All sequences were confirmed by Sanger (Quintarabio) and whole-plasmid (Primordium Labs) sequencing.

Cloning primers: (forward) 5'-CCGGGGGGAA-TGTGGCGGCGGAGGCAGCGACATCAAGCTG-CAGCA-3' (reverse) 5'-ATCTTATCATGTCTGGCCA-GCTAGCTCACTTCAGTTCCAGCTTTG-3'.

Cell culture

A549, A431, NCI-H441, SKBR3, Jurkat, and HEK293T cells were all purchased from the UCSF cell culture facility. A549, A431, NCI-H441, and SKBR3 cells were cultured and maintained in ATCC recommended conditions. HEK293T cells with Flag-CDCP1 overexpressed were generated according to literature (*63*). HEK293T cells with Flag-EGFR overexpressed were generated similarly. Jurkat cells expressing NFAT-GFP reporter were cultured in RPMI containing 10% FBS, 1% pen/strep, and 2 mg/ml geneticin.

K562-CD19 and Jurkat-CAR cells were cultured according to literature (*70*).

Mammalian protein expression

HEK293Expi (Expi293) cells were cultured in FreeStyle Expi293 media (Gibco, 12338018) at 37°C and 8% humidity with orbital shaking at 250 rpm. Protein expression plasmids were cloned into a pFUSE vector (InvivoGen) with upstream IL-2 secretion signal. Cells were transfected at 3M/ml density using FectoPRO transfection kit (Genesee Scientific, 55-332) according to manufacturers' instructions. After expression for 4-6 days, the supernatant from Expi293 cells was collected by centrifuging at 4000 g for 30 min and filtered through a 0.45 μm filter. After equilibrating Hitrap Protein A/L affinity column (GE Healthcare, 12-0402-01) or nickel resin, columns were washing with PBS (pH 7.4) using six times the column volume, and protein was eluted into 100 mM acetic acid. Following pH neutralization, the purified proteins were buffer exchanged with PBS (pH 7.4) using 10 kDa MW spin filters (AmiconUltra, UFC9010). Protein samples prepared in 4X loading dye with or without DTT were then characterized using SDS-PAGE. Purified proteins were quantified using A280 channel on a NanoDrop, and flash frozen in single use aliquots for storing at -80 °C or used fresh within a week.

General protocol for antibody conjugation with EY

In order to generate antibody-EY conjugates, different bioconjugation strategies were employed in Fig. 2 including NHS labeling and oxaziridine labeling. For NHS labeling, a 200 μl reaction mixture was prepared with final concentrations of 10 μM purified antibody and 50 μM N-Hydroxysuccinimidyl-4-azidobenzoate (NHS-azide, Lumiprobe, 63720) along with 10 mM sodium bicarbonate in PBS. The reaction was incubated for 1 hour at 25°C before another portion of NHS-azide was added to reach a final concentration 100 μM. The resulting mixture was allowed to react for additional 1 hour at 25°C. Then the conjugate was purified using a 7 kDa Zeba Spin desalting column (Thermo Scientific, 89882). The resulting azide-conjugated antibodies were then incubated with 100 μM DBCO-PEG_4-EY for 16 hours at 4 °C before purification with a 7 kDa Zeba Spin desalting column twice. Formation of the desired antibody-NHS-EY conjugates was confirmed by LC-MS, SDS-PAGE and UV-Vis spectrum scanning. The concentrations of proteins were calculated from SDS-PAGE gels. After characterization, the antibody-NHS-EY conjugate was flash frozen for future usage or used fresh within a week. For oxaziridine labeling, a 200 μl reaction was prepared with 10 μM purified antibody and 50 μM oxaziridine-azide (piperidine-oxaziridine 8 synthesized accordingly literature) (*35*) in PBS. The reaction was incubated for 1 hour at 25°C before purification using a 7 kDa Zeba Spin desalting column. The resulting azide-conjugated antibodies were then incubated with 50 μM DBCO-PEG_4-EY for 16 hours at 4°C before purification with a 7 kDa Zeba Spin desalting column twice. Formation of the desired antibody conjugate was confirmed as described above. After characterization, the corresponding antibody-Ox-EY conjugate was flash frozen for future usage or used fresh within a week.

Western blot protocol

Cells were incubated at 37°C in 5% CO_2 to 80% confluency and washed with 5 ml PBS three times before they were incubated with PBS with 0.04% EDTA (free of calcium and magnesium) for 15 min. Dissociated cells were collected and washed with 10 ml PBS three times before they were pelleted via centrifugation at 300 g for 5 min in 1.5 ml Eppendorf tubes. Cell pellets were resuspended in 1 ml 1X RIPA lysis buffer (EMD Millipore) supplemented with 1X cOmplete™ protease inhibitor cocktail (Roche). After 15 min incubation on ice, cells were sonicated for 15 s (5 s on, 5 s off, 20%). Cell lysates were then cleared by centrifugation at 20,000 g for 10 min at 4°C. Protein concentrations were measured using a BCA assay kit (Pierce). Samples were then analyzed by SDS-PAGE and transferred onto PVDF membranes using an iBlot2 transfer stack. Total protein was first assessed using Ponceau S staining. The membranes were then blocked using TBST with 5% BSA for 1 hour at 25°C before primary and secondary antibodies were added. Biotinylation and near-infrared Western blot imaging were conducted using an Odyssey Li-COR imaging system before further analysis using ImageStudioLite.

General flow cytometry

Cultured cells or coculture systems were incubated at 37°C in 5% CO_2 for the duration of the assay. Cells were first washed three times with 5 ml PBS followed by additional three washes with 5 ml filtered 3% BSA in PBS. Then the cells were either directly resuspended in 0.5 ml PBS for flow cytometry analysis or stained with corresponding primary antibody for 1 hour at 4°C. The stained cells were then washed three times with 5 ml filtered 3% BSA in PBS before they were resuspended in 0.5 ml PBS for flow cytometry analysis. Flow cytometry data were analyzed on FlowJo.

On-cell antibody binding and biotinylation assay

A431, A549 or NCI-H441 cells were incubated at 37°C in 5% CO_2 to 80% confluency and washed with PBS three times before they were incubated with PBS with 0.04% EDTA (free of calcium, magnesium) for 15 min. Dissociated cells were collected and washed three times with 10 ml PBS before they were pelleted in 1.5 ml Eppendorf tubes. Cells were resuspended in pre-chilled PBS to 1 X 10^6 cell/ml concentration, and then incubated with or without antibody or reagents as indicated at 4°C. Mixtures were illuminated with LED at 4°C, pelleted and washed again three times with 0.5 ml PBS. Treated cells were then stained with streptavidin-AlexaFluor488 (1:2000 diluted with filtered 3% BSA in PBS) and/or α-human IgG-AlexaFluor647 (1:2000 diluted with filtered 3% BSA in PBS) for 1 hour at 4°C before they were washed three times with 0.5 ml filtered 3% BSA in PBS. Samples were then suspended in 0.5 ml PBS before flow cytometry analysis.

Recombinant protein biotinylation assay

In order to test the catalytic function of EY when conjugated on an antibody, both self-labeling and target-biotinylation were validated using recombinant proteins. A 100 μl reaction system in PBS was prepared with 10 μM purified antibody or antibody-EY conjugate with or without equivalent amount of binding antigen for 15 min at 4°C. For example, 10 μM Ctx or Ctx-EY conjugate was incubated with or without 10 μM recombinant EGFR in PBS. Photo-probe (diazirine-biotin, aryl-azide-biotin, biocytin-hydrazide, or biotin-phenol) was then added into the solution to reach a final concentration of 100 μM and mixed thoroughly before illumination with LED for 10 min at 4°C. Afterwards, proteins were precipitated with pre-chilled acetone to get rid of excess small molecules, resuspended in PBS or sample loading buffer, and subjected to SDS-PAGE or LC-MS/MS sample preparation. Photo-probe modifications were searched as a dynamic modification with the following mass shift: diazirine-biotin (+ 616.25Da), aryl-azide-biotin (+ 620.23Da), phenol-biotin (+ 361.15Da) or biocytin-hydrazide (+ 384.50Da).

General protocol for antibody-EY labeling on cells

A431, A549, or NCI-H441 cells were incubated at 37°C in 5% CO_2 to 80% confluency and washed three times with PBS before they were incubated with PBS with 0.04% EDTA (free of calcium, magnesium) to dissociate. Dissociated cells were collected and washed with 5 ml PBS three times before they were pelleted in 1.5 ml Eppendorf tubes and resuspended in pre-chilled PBS to 10M cell/ml concentration. Indicated amounts of antibody-NHS-EY conjugates were pre-chilled and added to the cells for 15 min at 4°C before excessive antibody-EY conjugates were removed by washing with 1 ml pre-chilled PBS. The antibody-bound cells were then resuspended in 1 ml pre-chilled PBS. Photo-probe (diazirine-biotin, aryl-azide-biotin, biocytin-hydrazide, or biotin-phenol) was then added into the cell solution to reach a final concentration of 100 μM and mixed thoroughly before illumination with LED for 10 min at 4°C. Afterwards, cells were pelleted again and

subjected to flow cytometry or LC-MS/MS sample preparation.

Sample preparation for LC-MS/MS analysis

For sample processing, cell pellets were resuspended in 1 ml 1X RIPA lysis buffer (EMD Millipore) supplemented with 1X cOmplete™ protease inhibitor cocktail (Roche). After 15 min incubation on ice, cells were sonicated for 15 s (5 s on, 5 s off, 20%). Cell lysates were then cleared by centrifugation at 20,000 g for 10 min at 4 °C. Protein concentrations in the cleared supernatant were measured using a BCA assay kit (Pierce). Proteins were then added to 200 µl NeutrAvidin agarose beads (Pierce) that were pre-washed with 5 ml PBS for 3 times and incubated for 16 hours at 4 °C. Afterwards, supernatant was discarded using mini Bio-spin columns (Bio-Rad) and the beads were washed three times with 3 ml 1X RIPA lysis buffer, three times with 3 ml 1M NaCl in 1X PBS, and three time with 3 ml of freshly prepared 2M urea in 50 mM ammonium bicarbonate. The beads were then suspended in 100 µl PBS to re-constitute 50% slurry with 10 µl bead slurry separated for Western blotting.

Proteins on the washed beads were then digested using the Preomics iST kit in an on-bead digestion format according to the manufacturer's instructions. In brief, washed beads were suspended in 100 µl LYSE buffer provided by Preomics iST kit and incubated at 55°C for 10 min for reduction and alkylation. Once the beads cooled down to room temperature, 50 µl of pre-reconstituted DIGEST were added to the beads and incubated at 37°C for 3 hours with shaking. The digested peptides were then collected using mini Bio-Spin columns (Bio-Rad) and another 50 µl of LYSE buffer were added to wash the beads. Afterwards, 100 µl of STOP solution was added to the combined flow-through elution and mixed using vigorous vortexing. Then the peptides were desalted using the Preomics desalting columns before they were dried under vacuum and resuspended in 15 µl solvent A (0.1% formic acid with 2% acetonitrile) for mass spectrometry analysis. Peptide amount was monitored by quantitative fluorometric peptide assay (Pierce).

Proteomics analysis of digested peptide samples

Proteomics experiments were performed on a TimsTOF PRO (Bruker) equipped with a CaptiveSpray source and a nanoElute system. The peptides were separated on a 25 cm, ReproSil c18 1.5 µM 100 Å column (PepSep, PN. # PSC-25-150-15-UHP-nc) using a step-wise linear gradient method with water in 0.1% formic acid (solvent A) and acetonitrile with 0.1% formic acid (solvent B): 5-30% solvent B for 90 min at 0.5 µl/min, 30-35% solvent B for 10 min at 0.6 µl/min, 35-95% solvent B for 4 min at 0.5 µl/min, 95% hold for 4 min at 0.5 µl/min). Acquired data was collected in a data-dependent acquisition mode with ion mobility activated in PASEF mode. MS and MS/MS spectra were collected with m/z ranging from 100 to 1700 in positive mode.

Analysis of proteomics dataset

All acquired data was searched using PEAKS online Xpro 1.6 (Bioinformatics Solutions) or FragPipe powered by MSFragger (v3.7). Spectral searches were performed using a curated FASTA-formatted dataset containing Swiss Uniprot-reviewed human proteome file with gene ontology localized the plasma membrane (downloaded from UniProt database). A precursor mass error tolerance was set to 20 ppm and a fragment mass error tolerance was set at 0.03 ppm. Peptides, ranging from 6 to 45 amino acids in length, were searched in semi-specific trypsin digest mode with a maximum of three missed cleavages. Carbamidomethylation (+57.0214 Da) on cysteines was set as a static modification whereas methionine oxidation (+15.9949 Da) and lysine acetylation (+42.0115 Da) were set as a variable modification. Peptides were filtered based on a false discovery rate (FDR) of 1%. Samples were normalized using total ion current (TIC). For p-value and fold change calculations, the data were further processed using a customized script, as previously described (*71*). To analyze the portions of previously identified plasma membrane or cell surface proteins among the identified hits, annotated datasets were exported from UniProt or downloaded from previous reports (*72*, *73*).

Immunoprecipitation assays (co-IP) in live cells

For endogenous protein immunoprecipitation using protein A/G beads, cell lysates with equal amounts of protein were diluted with PBS and incubated with protein A/G beads (pre-washed three times with binding buffer, 50 mM Tris, 150 mM NaCl, 0.2% Triton, pH = 7.5) for 2 hours at 4°C along with the protein-specific antibody at the vendor-suggested dilution. The beads were washed three times with binding buffer (50 mM Tris, 150 mM NaCl, 0.2% Triton, pH = 7.5). The enriched proteins were eluted with acidic elution buffer (100 mM glycine, 0.1% Triton, pH 2.8) before neutralizing with 1M Tris (pH 8), according to the manufacturer's instructions.

AlphaFold-Multimer prediction and analysis

We performed in silico screening using AlphaFold-Multimer program on the ColabFold platform as previously described (*25*, *74*, *75*). In brief, AlphaFold-Multimer calculations were performed using AlphaFold-Multimer v3 on ColabFold v1.5.2 (*58*, *76*) using NVIDIA A100 GPUs with sequence alignment generated through MMseqs2 and HHsearch. Predictions were generated in a combination of the paired and unpaired multiple sequence alignment, 20 recycles to generate 5 independent unrelaxed models. Sequences were obtained directly from UniProt database. All ranks are examined by both prediction confidence and accuracy. Models with an average predicted local distance difference threshold (pLDDT)>50 and minimum predicted alignment error (PAE) < 15 Å were considered (*56*).

Predicted AlphaFold-Multimer binary complexes were further scored using predicted DockQ score (pDockQ) and buried solvent accessible surface area (BSASA). pDockQ scores were generated to indicate the interface accuracy quantitatively (0 is the worst and 1 is the best) with ≥0.23 cutoff value for direct binary contact as previously described (*58*). BSASA is defined as $\Delta SASA_{AB} = SASA_A + SASA_B - SASA_{AB}$, where a 1.4 Å radii rolling probe was used to calculate solvent accessible surface area for all non-hydrogen, non-monoatomic ion atoms in chains A and B (*59*, *60*, *77*).

Preparation of cell-cell synapses using cocultured cells.

In order to activate cell-cell recognition, a mixture of two cells were prepared and counted. In the case of BiTE systems, target cell line (HEK293T-Flag-EGFR, HEK293T-Flag-CDCP1, SKBR3) were first plated and let attach to the plate for 8 hours. Jurkat NFAT-GFP was then added at a 2.5:1 effector: target ratio. Indicated concentration of BiTE or BiTE-EY construct was added and incubated for more than 20 hours before the cells were harvested for flow cytometry or on-cell biotinylation experiments. In the case of the CAR system, Jurkat-CAR and K562-CD19 were plated at a 2.5:1 effector: target ratio and incubated for 20 hours before the cells were harvested for flow cytometry or on-cell biotinylation experiments.

Cell-cell biotinylation sample preparation

For intercellular biotinylation experiments, cocultured cells were carefully washed with pre-chilled PBS. Indicated amounts of pre-chilled antibody-EY were added to the cells for 15 min at 4°C. Photo-probe (diazirine-biotin, aryl-azide-biotin, biocytin-hydrazide, or biotin-phenol) was then added into the samples and mixed thoroughly before LED illumination for 10 min at 4°C. Afterwards, cells were pelleted and wash three times with PBS. The cells were either lysed directly for LC-MS/MS sample preparation as described above or FACS sorted before sample preparation. To perform FACS sorting, cells were stained with α-CD3-AlexaFluor561 before they were sorted into $CD3^+$ and $CD3^-$ cells using a Sony cell sorter (SH800S).

Cell-cell biotinylation confocal imaging

Cell-cell synapses were prepared and biotinylated on an iBidi plate precoated with ibiTreat (µ-Dish 35 mm, iBidi 81156). Treated cells were gently washed twice with PBS before freshly diluted 4%

paraformaldehyde was added dropwise. Cells were fixed for 10 min at 25°C and gently washed twice with PBS. Freshly filtered 3% BSA in PBS was then added dropwise to block for 8 hours at 4°C. Cells were stained with streptavidin-AlexaFluor647 (dilution 1:1000 diluted with filtered 3% BSA in PBS) for 1 hour at 4°C in dark, gently washed twice with PBS and stained with freshly diluted Hoechst DNA dye for 10 min at 25°C in dark. The samples were again gently washed twice with PBS and imaged with an inverted Nikon Ti-E microscope equipped with a Yokogawa CSU-22 confocal scanner unit.

Software

Data were analyzed and visualized using Microsoft Excel (v16.22) and GraphPad Prism (v8.0.1), in addition to software listed by each experiment. NMR data were analyzed using MestReNova (v15.0.0). DNA and protein sequences were analyzed using Geneious (v10.0.7). Flow cytometry data were analyzed by FlowJo (v10.6.1) and FACS data were processed by Software Wizards installed on SH800S cell sorter. Proteomics data were analyzed by PEAKS online (Xpro 1.6) and FragPipe powered by MSFragger (v3.7). Images were made using ImageStudioLite (v5.2.5), Adobe Illustrator (v22.1) and BioRender (v2.0). Structural assignments to site-specific modifications and structural comparison were performed using ChimeraX (v1.6.1). AlphaFold-Multimer prediction was performed on ColabFold (v1.5.2) and visualized using ChimeraX (v1.6.1). Code for BSASA calculation is publicly available on GitHub and Dryad: https://github.com/ajipalar/guide_bsasa (commit 7541e6f3ba89a0089b7f01c8792a2f356264cd68).

Statistical analysis

Statistical analyses (unpaired Student's *t* tests) were performed using GraphPad Prism. Data were derived from at least three biological replicate experiments and presented as the mean ± s.d., $P \leq 0.05$, $^{**}P \leq 0.01$, $^{***}P \leq 0.001$, $^{****}P \leq 0.0001$ and n.s., not significant.

REFERENCES AND NOTES

1. M. Uhlén *et al*., The human secretome. *Sci. Signal.* **12**, eaaz0274 (2019). doi: 10.1126/scisignal.aaz0274; pmid: 31772123
2. D. H. Siepe *et al*., Identification of orphan ligand-receptor relationships using a cell-based CRISPRa enrichment screening platform. *eLife* **11**, e81398 (2022). doi: 10.7554/eLife.81398; pmid: 36178190
3. C. C. Wu, J. R. Yates 3rd, The application of mass spectrometry to membrane proteomics. *Nat. Biotechnol.* **21**, 262–267 (2003). doi: 10.1038/nbt0303-262; pmid: 12610573
4. N. P. Barrera, C. V. Robinson, Advances in the mass spectrometry of membrane proteins: From individual proteins to intact complexes. *Annu. Rev. Biochem.* **80**, 247–271 (2011). doi: 10.1146/annurev-biochem-062309-093307; pmid: 21548785
5. W. Qin, K. F. Cho, P. E. Cavanagh, A. Y. Ting, Deciphering molecular interactions by proximity labeling. *Nat. Methods* **18**, 133–143 (2021). doi: 10.1038/s41592-020-01010-5; pmid: 33432242
6. C. P. Seath, A. D. Trowbridge, T. W. Muir, D. W. C. MacMillan, Reactive intermediates for interactome mapping. *Chem. Soc. Rev.* **50**, 2911–2926 (2021). doi: 10.1039/D0CS01366H; pmid: 33458734
7. S. S. Lam *et al*., Directed evolution of APEX2 for electron microscopy and proximity labeling. *Nat. Methods* **12**, 51–54 (2015). doi: 10.1038/nmeth.3179; pmid: 25419960
8. K. J. Roux, D. I. Kim, B. Burke, D. G. May, BioID: A Screen for Protein-Protein Interactions. *Curr. Protoc. Protein Sci.* **91**, 23.1, 15 (2018). doi: 10.1002/cpps.51; pmid: 29516480
9. T. C. Branon *et al*., Efficient proximity labeling in living cells and organisms with TurboID. *Nat. Biotechnol.* **36**, 880–887 (2018). doi: 10.1038/nbt.4201; pmid: 30125270
10. W. Qin *et al*., Dynamic mapping of proteome trafficking within and between living cells by TransitID. *Cell* **186**, 3307–3324.e30 (2023). doi: 10.1016/j.cell.2023.05.044; pmid: 37385249
11. J. V. Oakley *et al*., Radius measurement via super-resolution microscopy enables the development of a variable radii proximity labeling platform. *Proc. Natl. Acad. Sci. U.S.A.* **119**, e2203027119 (2022). doi: 10.1073/pnas.2203027119; pmid: 35914173
12. M. Müller *et al*., Light-mediated discovery of surfaceome nanoscale organization and intercellular receptor interaction networks. *Nat. Commun.* **12**, 7036 (2021). doi: 10.1038/s41467-021-27280-x; pmid: 34857745
13. M. K. Kuimova, G. Yahioglu, P. R. Ogilby, Singlet oxygen in a cell: Spatially dependent lifetimes and quenching rate constants. *J. Am. Chem. Soc.* **131**, 332–340 (2009). doi: 10.1021/ja807484b; pmid: 19128181
14. M. Lindén, P. Sens, R. Phillips, Entropic tension in crowded membranes. *PLOS Comput. Biol.* **8**, e1002431 (2012). doi: 10.1371/journal.pcbi.1002431; pmid: 22438801
15. J. B. Geri *et al*., Microenvironment mapping via Dexter energy transfer on immune cells. *Science* **367**, 1091–1097 (2020). doi: 10.1126/science.aay4106; pmid: 32139536
16. T. J. Bechtel, T. Reyes-Robles, O. O. Fadeyi, R. C. Oslund, Strategies for monitoring cell-cell interactions. *Nat. Chem. Biol.* **17**, 641–652 (2021). doi: 10.1038/s41589-021-00790-x; pmid: 34035514
17. R. C. Oslund *et al*., Detection of cell-cell interactions via photocatalytic cell tagging. *Nat. Chem. Biol.* **18**, 850–858 (2022). doi: 10.1038/s41589-022-01044-0; pmid: 35654846
18. D. C. Cabanero *et al*., Photocatalytic activation of aryl (trifluoromethyl) diazos to carbenes for high-resolution protein labeling with red light. *J. Am. Chem. Soc.* **146**, 1337–1345 (2024). doi: 10.1021/jacs.3c09545; pmid: 38165744
19. B. A. G. DeGraff, D. W. Gillespie, R. J. Sundberg, Phenyl nitrene: A flash photolytic investigation of the reaction with secondary amines. *J. Am. Chem. Soc.* **95**, 7491–7496 (1973).
20. T. G. Bartholow *et al*., Photoproximity labeling from single catalyst sites allows calibration and increased resolution for carbene labeling of protein partners in vitro and on cells. *ACS Cent. Sci.* **10**, 199–208 (2023). doi: 10.1021/acscentsci.3c01473; pmid: 38292613
21. B. F. Buksh *et al*., μMap-Red: Proximity labeling by red light photocatalysis. *J. Am. Chem. Soc.* **144**, 6154–6162 (2022). doi: 10.1021/jacs.2c01384; pmid: 35363468
22. N. E. S. Tay *et al*., Targeted activation in localized protein environments via deep red photoredox catalysis. *Nat. Chem.* **15**, 101–109 (2023). pmid: 36216892
23. T. Reyes-Robles *et al*., Nanoscale mapping of EGFR and c-MET protein environments on lung cancer cell surfaces via therapeutic antibody photocatalyst conjugates. *ACS Chem. Biol.* **17**, 2304–2314 (2022). doi: 10.1021/acschembio.2c00409; pmid: 35939534
24. T. J. Bechtel *et al*., Proteomic mapping of intercellular synaptic environments *via* flavin-dependent photoredox catalysis. *Org. Biomol. Chem.* **21**, 98–106 (2022). doi: 10.1039/D2OB02103J; pmid: 36477737
25. R. Evans *et al*., Protein complex prediction with AlphaFold-Multimer. biorxiv 463034 [Preprint] (2022); https://doi.org/10.1101/2021.10.04.463034.
26. A. J. Slezak *et al*., Tumor cell-surface binding of immune stimulating polymeric glyco-adjuvant via cysteine-reactive pyridyl disulfide promotes antitumor immunity. *ACS Cent. Sci.* **8**, 1435–1446 (2022). doi: 10.1021/acscentsci.2c00704; pmid: 36313164
27. M. Majek, A. Jacobi von Wangelin, Mechanistic perspectives on organic photoredox catalysis for aromatic substitutions. *Acc. Chem. Res.* **49**, 2316–2327 (2016). doi: 10.1021/acs.accounts.6b00293; pmid: 27669097
28. N. E. S. Tay *et al*., Targeted activation in localized protein environments via deep red photoredox catalysis. *Nat. Chem.* **15**, 101–109 (2023). doi: 10.1038/s41557-022-01057-1; pmid: 36216892
29. Z. Huang *et al*., Bioorthogonal photocatalytic decaging-enabled mitochondrial proteomics. *J. Am. Chem. Soc.* **143**, 18714–18720 (2021). doi: 10.1021/jacs.1c09171; pmid: 34709827
30. Y. Fang, P. Zou, Photocatalytic proximity labeling for profiling the subcellular organization of biomolecules. *ChemBioChem* **24**, e202200745 (2023). doi: 10.1002/cbic.202200745; pmid: 36762434
31. K. Toh *et al*., Chemoproteomic identification of blue-light-damaged proteins. *J. Am. Chem. Soc.* **144**, 20171–20176 (2022). doi: 10.1021/jacs.2c07180; pmid: 36306265
32. S. Lin *et al*., Redox-based reagents for chemoselective methionine bioconjugation. *Science* **355**, 597–602 (2017). doi: 10.1126/science.aal3316; pmid: 28183972
33. S. Li *et al*., Structural basis for inhibition of the epidermal growth factor receptor by cetuximab. *Cancer Cell* **7**, 301–311 (2005). doi: 10.1016/j.ccr.2005.03.003; pmid: 15837620
34. K. Yonesaka *et al*., Activation of ERBB2 signaling causes resistance to the EGFR-directed therapeutic antibody cetuximab. *Sci. Transl. Med.* **3**, 99ra86 (2011). doi: 10.1126/scitranslmed.3002442; pmid: 21900593
35. S. K. Elledge *et al*., Systematic identification of engineered methionines and oxaziridines for efficient, stable, and site-specific antibody bioconjugation. *Proc. Natl. Acad. Sci. U.S.A.* **117**, 5733–5740 (2020). doi: 10.1073/pnas.1920561117; pmid: 32123103
36. D. I. Kim, K. J. Roux, Filling the Void: Proximity-based labeling of proteins in living cells. *Trends Cell Biol.* **26**, 804–817 (2016). doi: 10.1016/j.tcb.2016.09.004; pmid: 27667171
37. A. V. West *et al*., Labeling preferences of diazirines with protein biomolecules. *J. Am. Chem. Soc.* **143**, 6691–6700 (2021). doi: 10.1021/jacs.1c02509; pmid: 33876925
38. H. Wang *et al*., Selective mitochondrial protein labeling enabled by biocompatible photocatalytic reactions inside live cells. *JACS Au* **1**, 1066–1075 (2021). doi: 10.1021/jacsau.1c00172; pmid: 34467350
39. H. Kimura *et al*., Antibody-dependent cellular cytotoxicity of cetuximab against tumor cells with wild-type or mutant epidermal growth factor receptor. *Cancer Sci.* **98**, 1275–1280 (2007). doi: 10.1111/j.1349-7006.2007.00510.x; pmid: 17498200
40. H. Masui, L. Castro, J. Mendelsohn, Consumption of EGF by A431 cells: Evidence for receptor recycling. *J. Cell Biol.* **120**, 85–93 (1993). doi: 10.1083/jcb.120.1.85; pmid: 8416997
41. J. R. Wiśniewski, M. Y. Hein, J. Cox, M. Mann, A "proteomic ruler" for protein copy number and concentration estimation without spike-in standards. *Mol. Cell. Proteomics* **13**, 3497–3506 (2014). doi: 10.1074/mcp.M113.037309; pmid: 25225357
42. Z. Yao *et al*., A global analysis of the receptor tyrosine kinase-protein phosphatase interactome. *Mol. Cell* **65**, 347–360 (2017). doi: 10.1016/j.molcel.2016.12.004; pmid: 28065597
43. S. Foerster *et al*., Characterization of the EGFR interactome reveals associated protein complex networks and intracellular receptor dynamics. *Proteomics* **13**, 3131–3144 (2013). doi: 10.1002/pmic.201300154; pmid: 23956138
44. J. Li *et al*., Perturbation of the mutated EGFR interactome identifies vulnerabilities and resistance mechanisms. *Mol. Syst. Biol.* **9**, 705 (2013). doi: 10.1038/msb.2013.61; pmid: 24189400
45. V. Morello *et al*., β1 integrin controls EGFR signaling and tumorigenic properties of lung cancer cells. *Oncogene* **30**, 4087–4096 (2011). doi: 10.1038/onc.2011.107; pmid: 21478906
46. M. Petrás *et al*., Molecular interactions of ErbB1 (EGFR) and integrin-β1 in astrocytoma frozen sections predict clinical outcome and correlate with Akt-mediated in vitro radioresistance. *Neuro-oncol.* **15**, 1027–1040 (2013). doi: 10.1093/neuonc/not046; pmid: 23595626
47. Y. Zheng *et al*., Secreted and O-GlcNAcylated MIF binds to the human EGF receptor and inhibits its activation. *Nat. Cell Biol.* **17**, 1348–1355 (2015). doi: 10.1038/ncb3222; pmid: 26280537
48. T. Okamura *et al*., Tyrosine phosphorylation of the human glutathione *S*-transferase P1 by epidermal growth factor receptor. *J. Biol. Chem.* **284**, 16979–16989 (2009). doi: 10.1074/jbc.M808153200; pmid: 19254954
49. T. Kaihara *et al*., Redifferentiation and ZO-1 reexpression in liver-metastasized colorectal cancer: Possible association with epidermal growth factor receptor-induced tyrosine phosphorylation of ZO-1. *Cancer Sci.* **94**, 166–172 (2003). doi: 10.1111/j.1349-7006.2003.tb01414.x; pmid: 12708492
50. S. Meran *et al*., Hyaluronan facilitates transforming growth factor-β1-dependent proliferation via CD44 and epidermal growth factor receptor interaction. *J. Biol. Chem.* **286**, 17618–17630 (2011). doi: 10.1074/jbc.M111.226563; pmid: 21454519
51. G. D. Grass, L. B. Tolliver, M. Bratoeva, B. P. Toole, CD147, CD44, and the epidermal growth factor receptor (EGFR) signaling pathway cooperate to regulate breast epithelial cell invasiveness. *J. Biol. Chem.* **288**, 26089–26104 (2013). doi: 10.1074/jbc.M113.497685; pmid: 23888049

52. J. Merlin *et al*., Galectin-3 regulates MUC1 and EGFR cellular distribution and EGFR downstream pathways in pancreatic cancer cells. *Oncogene* **30**, 2514–2525 (2011). doi: 10.1038/onc.2010.631; pmid: 21258405
53. M. Ferrandi *et al*., Adducin- and ouabain-related gene variants predict the antihypertensive activity of rostafuroxin, part 1: Experimental studies. *Sci. Transl. Med.* **2**, 59ra86 (2010). doi: 10.1126/scitranslmed.3001815; pmid: 21106940
54. E. C. Stites, The response of cancers to BRAF inhibition underscores the importance of cancer systems biology. *Sci. Signal.* **5**, pe46 (2012). doi: 10.1126/scisignal.2003354; pmid: 23074264
55. C. Y. Chen *et al*., Tid1-L inhibits EGFR signaling in lung adenocarcinoma by enhancing EGFR Ubiquitinylation and degradation. *Cancer Res.* **73**, 4009–4019 (2013). doi: 10.1158/0008-5472.CAN-12-4066; pmid: 23698466
56. Y. Lim *et al*., In silico protein interaction screening uncovers DONSON's role in replication initiation. *Science* **381**, eadi3448 (2023). doi: 10.1126/science.adi3448; pmid: 37590370
57. X. Gu *et al*., The midnolin-proteasome pathway catches proteins for ubiquitination-independent degradation. *Science* **381**, eadh5021 (2023). doi: 10.1126/science.adh5021; pmid: 37616343
58. P. Bryant, G. Pozzati, A. Elofsson, Improved prediction of protein-protein interactions using AlphaFold2. *Nat. Commun.* **13**, 1265 (2022). doi: 10.1038/s41467-022-28865-w; pmid: 35273146
59. A. Shrake, J. A. Rupley, Environment and exposure to solvent of protein atoms. Lysozyme and insulin. *J. Mol. Biol.* **79**, 351–371 (1973). doi: 10.1016/0022-2836(73)90011-9; pmid: 4760134
60. F. P. Davis, A. Sali, PIBASE: A comprehensive database of structurally defined protein interfaces. *Bioinformatics* **21**, 1901–1907 (2005). doi: 10.1093/bioinformatics/bti277; pmid: 15657096
61. H. Ogiso *et al*., Crystal structure of the complex of human epidermal growth factor and receptor extracellular domains. *Cell* **110**, 775–787 (2002). doi: 10.1016/S0092-8674(02)00963-7; pmid: 12297050
62. E. N. Banhos Danneskiold-Sams *et al*., Rapid and accurate deorphanization of ligand-receptor pairs using AlphaFold. bioRxiv 531341 [Preprint] (2023); https://doi.org/10.1101/2023.03.16.531341.
63. S. A. Lim *et al*., Targeting a proteolytic neoepitope on CUB domain containing protein 1 (CDCP1) for RAS-driven cancers. *J. Clin. Invest.* **132**, e154604 (2022). doi: 10.1172/JCI154604; pmid: 35166238
64. F. Macian, NFAT proteins: Key regulators of T-cell development and function. *Nat. Rev. Immunol.* **5**, 472–484 (2005). doi: 10.1038/nri1632; pmid: 15928679
65. J. S. Klein *et al*., Examination of the contributions of size and avidity to the neutralization mechanisms of the anti-HIV antibodies b12 and 4E10. *Proc. Natl. Acad. Sci. U.S.A.* **106**, 7385–7390 (2009). doi: 10.1073/pnas.0811427106; pmid: 19372381
66. Q. Xiao *et al*., Size-dependent activation of CAR-T cells. *Sci. Immunol.* **7**, eabl3995 (2022). doi: 10.1126/sciimmunol.abl3995; pmid: 35930653
67. L. D. Lavis, Teaching old dyes new tricks: Biological probes built from fluoresceins and rhodamines. *Annu. Rev. Biochem.* **86**, 825–843 (2017). doi: 10.1146/annurev-biochem-061516-044839; pmid: 28399656
68. D. P. Hari, B. König, Synthetic applications of eosin Y in photoredox catalysis. *Chem. Commun.* **50**, 6688–6699 (2014). doi: 10.1039/C4CC00751D; pmid: 24699920
69. N. H. Cho *et al*., OpenCell: Endogenous tagging for the cartography of human cellular organization. *Science* **375**, eabi6983 (2022). doi: 10.1126/science.abi6983; pmid: 35271311
70. J. R. Klesmith *et al*., Retargeting CD19 chimeric antigen receptor T cells via engineered CD19-fusion proteins. *Mol. Pharm.* **16**, 3544–3558 (2019). doi: 10.1021/acs.molpharmaceut.9b00418; pmid: 31242389
71. Y. Ge *et al*., Target protein deglycosylation in living cells by a nanobody-fused split O-GlcNAcase. *Nat. Chem. Biol.* **17**, 593–600 (2021). doi: 10.1038/s41589-021-00757-y; pmid: 33686291
72. Y. Li *et al*., Rapid enzyme-mediated biotinylation for cell surface proteome profiling. *Anal. Chem.* **93**, 4542–4551 (2021). doi: 10.1021/acs.analchem.0c04970; pmid: 33660993
73. D. Bausch-Fluck *et al*., The in silico human surfaceome. *Proc. Natl. Acad. Sci. U.S.A.* **115**, E10988–E10997 (2018). doi: 10.1073/pnas.1808790115; pmid: 30373828
74. Z. C. Drake, J. T. Seffernick, S. Lindert, Protein complex prediction using Rosetta, AlphaFold, and mass spectrometry covalent labeling. *Nat. Commun.* **13**, 7846 (2022). doi: 10.1038/s41467-022-35593-8; pmid: 36543826
75. J. Jumper *et al*., Highly accurate protein structure prediction with AlphaFold. *Nature* **596**, 583–589 (2021). doi: 10.1038/s41586-021-03819-2; pmid: 34265844
76. M. Mirdita *et al*., ColabFold: Making protein folding accessible to all. *Nat. Methods* **19**, 679–682 (2022). doi: 10.1038/s41592-022-01488-1; pmid: 35637307
77. P. Kunzmann, K. Hamacher, Biotite: A unifying open source computational biology framework in Python. *BMC Bioinformatics* **19**, 346 (2018). doi: 10.1186/s12859-018-2367-z; pmid: 30285630
78. Z. Lin *et al*., Multiscale photocatalytic proximity labeling reveals cell surface neighbors on and between cells. Dryad (2024). https://doi.org/10.5061/dryad.j6q573nmq.

ACKNOWLEDGEMENTS

We thank J. Zhou, K. Leung, T. Bartholow, J. Maza, K. Kumru, C. Delaveris, P. Burroughs, and J. Byrnes for insightful discussions. We also thank S. Elledge for the Her2 Fab expression plasmids, J. Duque-Jimenez and X. Zhou from Harvard Medical School for CAR-T and K562-CD19 cells, as well as J. Yu from Harvard Medical School for guidance in conducting the AlphaFold-Multimer analysis. **Funding:** We are grateful to generous support from NIH (1R01CA248323-01). K.S. is a Merck fellow of the Helen Hay Whitney Foundation. Z.Y. is supported by an NIH National Institute of General Medical Sciences F32 grant (1F32GM149084-01). A.S. is supported by NIH (P41GM109824 and R01GM083960). A.P. is supported by NIH (U19AI135990). The HDFCC LCA for cell sorting is funded by NIH (P30CA082103). **Author contributions:** Z.L. and J.A.W. designed the project, analyzed the data, and wrote the manuscript, with input from all authors. K.S. and Z.Y. generated plasmids and purified proteins. I.L. assisted the cell sorting experiments. A.F. and D.L.S. assisted the MS experiments. A.P. and A.S. assisted AlphaFold-Multimer analysis and BSASA calculation. **Competing interests:** The authors declare the following competing financial interests: J.A.W. and Z.L. filed a provisional patent on the multiscale interactome profiling of membrane proteins using photocatalytic proximity labeling (The Regents of the University of California, 63/472,087). D.L.S. has a financially compensated consulting agreement with Maze Therapeutics and Rezo Therapeutics. J.A.W. is a member of the Board of Directors and Scientific Advisory Board (SAB) for EpiBiologics and SAB for Crossbow Therapeutics, IgGenix Therapeutics, Spotlight Therapeutics, Jnana Therapeutics, RedTree Ventures, and Inception. J.A.W. is a consultant for Arena Bioworks. **Data and materials availability:** All data are available in the main text or the supplementary materials. The MS proteomics data have been deposited to the ProteomeXchange Consortium through the PRIDE partner repository with the dataset identifier PXD051348. Customized script for AlphaFold-Multimer assessment and prediction coordinates are described in the Materials and methods section and deposited to Dryad along with uncropped blots (*78*).

SUPPLEMENTARY MATERIALS

science.org/doi/10.1126/science.adl5763
Figs. S1 to S14
Tables S1 to S19
MDAR Reproducibility Checklist

Submitted 29 October 2023; accepted 10 June 2024
10.1126/science.adl5763